Journal of Nanobiotechnology

RESEARCH

Open Access

CREB1/CRTC2 regulated tubular epithelial-derived exosomal miR-93-3p promotes kidney injury induced by calcium oxalate via activating M1 polarization and macrophage extracellular trap formation

Yushi Sun[1†], Bojun Li[1†], Baofeng Song[1†], Yuqi Xia[1], Xiangjun Zhou[1], Fangyou Lin[1*†], Ting Rao[1*†] and Fan Cheng[1*†]

Abstract

Background Calcium oxalate (CaOx) crystals are known to cause renal injury and trigger inflammatory responses. However, the role of exosome-mediated epithelial-macrophage communication in CaOx-induced kidney injury remains unclear.

Methods To identify key molecules, miRNA sequencing was conducted on exosomes derived from CaOx-treated (CaOx-exo) and control (Ctrl-exo) epithelial cells, identifying miR-93-3p as significantly upregulated. A combination of dual-luciferase reporter assays, Western blot, RT-qPCR, immunofluorescence staining, flow cytometry, electrophoretic mobility shift assay (EMSA), and chromatin immunoprecipitation-qPCR (CHIP-qPCR) was used to explore the regulation of miR-93-3p by CREB1/CRTC2 and its downstream effects on NFAT5/Akt1/NIK/NF-κB2 signaling in macrophages. The functional roles of NFAT5 in macrophage polarization and macrophage extracellular traps (METs) formation were further evaluated both in vitro and in vivo.

Results Epithelial exosomes stimulated by CaOx crystals were found to promote kidney injury via macrophage polarization and METs formation. Treatment with NIK SMI1, a NIK inhibitor, or Cl-amidine, a METs inhibitor, mitigated crystal deposition and CaOx-induced kidney damage. Overexpression of NFAT5 in a CaOx-induced mouse model reduced renal injury and crystal deposition, downregulated NIK and NF-κB2 levels, and decreased the number of

[†]Yushi Sun, Bojun Li and Baofeng Song contributed equally to this work.

[†]Fangyou Lin, Ting Rao and Fan Cheng contributed equally to this work.

*Correspondence:
Fangyou Lin
141548237@qq.com
Ting Rao
tinart@126.com
Fan Cheng
urology1969@aliyun.com

Full list of author information is available at the end of the article

M1-polarized macrophages. Mechanistic studies revealed that miR-93-3p directly targets NFAT5 mRNA, as confirmed by dual-luciferase assays, qRT-PCR, and Western blot. Additionally, we demonstrated that CREB1/CRTC2 acts as a transcriptional activator of miR-93-3p. Inhibition of miR-93-3p partially reversed NIK/NF-κB2 activation and alleviated kidney injury.

Conclusions CaOx crystals exacerbate renal interstitial injury by promoting M1 macrophage polarization and METs formation through the CREB1/CRTC2–exosomal miR-93-3p–NIK/NF-κB2 signaling pathway. Targeting this pathway may provide therapeutic avenues for mitigating crystal deposition-induced kidney damage.

Keywords Kidney stones, Exosomes, miR-93-3p, Macrophages, NIK/NF-κB2, Macrophage extracellular traps

Introduction

Kidney calculi represent a prevalent urological disorder, with epidemiological studies indicating a 1.0-5.0% incidence rate in China and a progressive upward trend [1]. Calcium-containing stones, predominantly composed of calcium oxalate (CaOx), constitute approximately 80% renal calculi [2, 3]. The renal susceptibility to crystal formation leads to various crystal nephropathies, primarily through CaOx-induced cytotoxicity in renal tubular epithelial cells. This cytotoxicity manifests through mitochondrial dysfunction, elevated reactive oxygen species (ROS) production, lysosomal impairment, and inflammasome activation [4, 5]. Subsequent cytokine release from necrotic cells amplifies renal inflammation, potentially triggering acute kidney injury and accelerating CaOx crystal retention.

The deposition of CaOx crystals in renal interstitium triggers macrophage migration and activation. Activated macrophages release chemotactic factors that mobilize circulating monocytes to differentiate into tissue macrophages at deposition sites, aiming to engulf and degrade the crystal deposits over time [6, 7]. As important immune cells, macrophages exhibit functional plasticity [8], differentiating into classically activated (M1) or alternatively activated (M2) phenotypes under specific stimuli [9, 10]. Evidence from numerous studies suggests that long-term exposure to CaOx promotes M1 polarization, characterized by pro-inflammatory cytokine secretion (IL-6, IFN-γ, TNF-α) and adhesion molecule expression (VCAM-1), thereby propagating inflammatory cascades that facilitate stone formation [11–13]. In addition to their classical phagocytic and digestive functions, macrophages, like neutrophils, can also act produce a network of granular proteins and DNA called macrophage extracellular traps (METs), in response to specific stimuli [14, 15]. METs play a crucial role in anti-infective immunity by capturing and neutralizing pathogens to prevent their spread. In addition, METs is the core structure of macrophages regulating inflammation and related cellular mechanisms [16]. Despite their established roles in immunity, the impact of METs on kidney stone formation and renal injury remain unclear.

Recent studies have shown that extracellular vesicles (EVs), particularly exosomes (30–120 nm vesicles derived from multivesicular body-plasma membrane fusion), as critical mediators of intercellular communication [17, 18]. These nanovesicles transport bioactive cargo (cytokines, microRNAs, membrane receptors) to modulate recipient cell physiology [19, 20]. Their involvement spans diverse pathophysiological processes including immune regulation and tissue injury [21, 22]. Our prior work identified CaOx-stimulated renal epithelial exosomes as drivers of M1 macrophage polarization via microRNA transfer [23]. Here, we aim to delve deeper into the molecular mechanisms of exosome-mediated macrophage reprogramming underlying this process.

Clinical observations reveal elevated urinary exosome levels in nephrolithiasis patients, enriched with inflammatory mediators and noncoding RNAs [24]. Our pioneering study elucidates how renal tubular epithelial cell (RTEC)-derived exosomes deliver genetic regulators to macrophages, establishing a pro-inflammatory microenvironment conducive to crystal retention. This exosome-mediated RTEC-macrophage crosstalk represents a novel therapeutic target for mitigating stone-related renal injury.

Results

Macrophage infiltration was increased in kidney tissue of CaOx crystal deposition mice and stone patients

We established a mouse model using a vitamin D-supplemented high-calcium diet (Fig. 1A) according to previously reported methods [25]. Blood urea nitrogen (BUN) and serum creatinine (Scr) levels, and urinary calcium and oxalate levels increased were increased remarkably in this model (Fig. 1B). HE and Von Kossa staining indicated an aggravated renal cortical injury and increased calcium crystal deposition in renal tubular lumens (Fig. 1C-D), suggesting the successful establishment of the mouse model of nephrolithiasis. Tunel and F4/80 staining demonstrated the enhanced macrophage infiltration in the kidneys of nephrolithiasis mice (Fig. 1C-D). MCP-1, IL-6 and TNF-α were significantly up-regulated in kidney stone mice (Fig. 1E). The immunohistochemical positive level of CD68 in the kidney tissue of nephrolithiasis

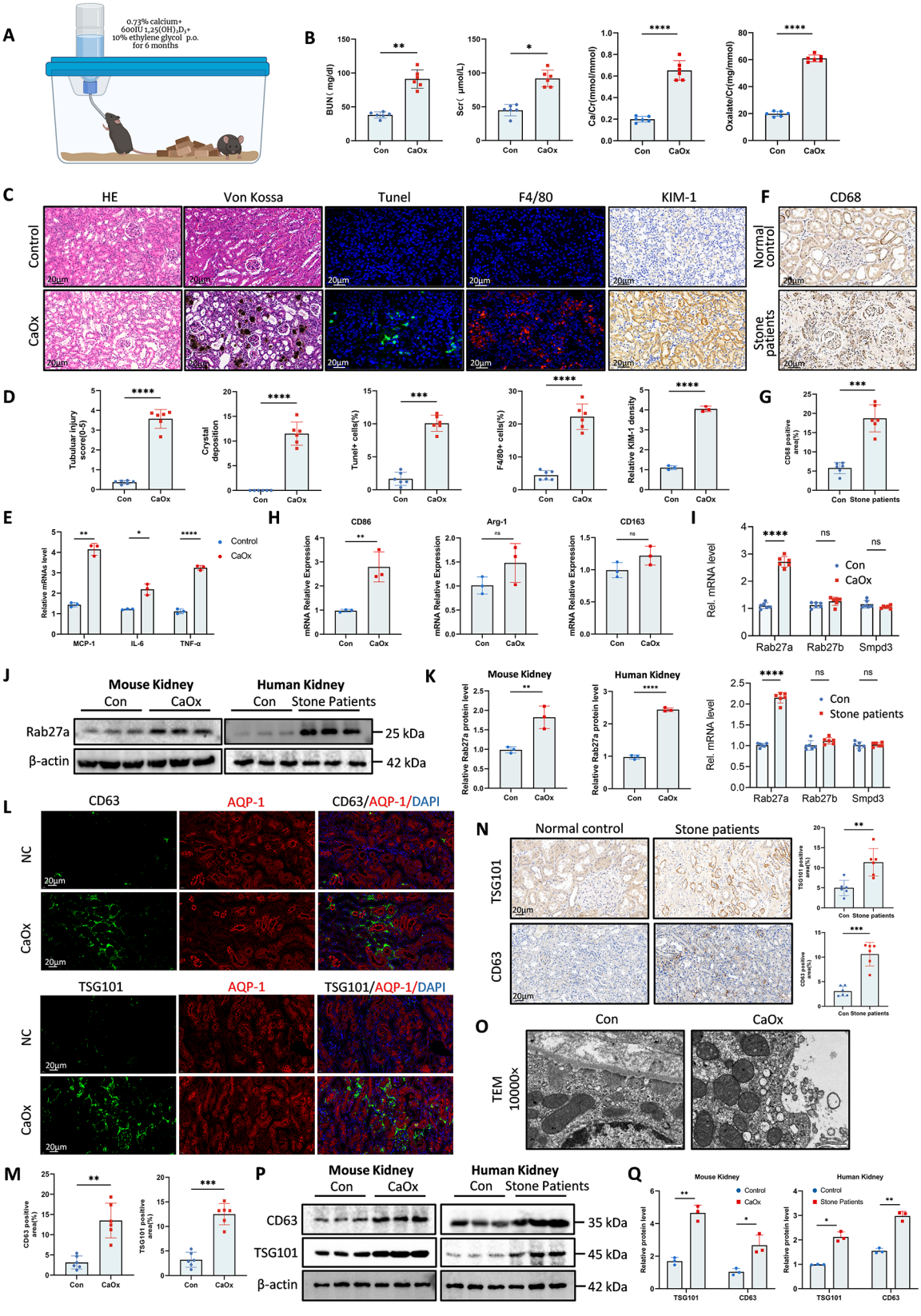

Fig. 1 (See legend on next page.)

(See figure on previous page.)

Fig. 1 Macrophage infiltration and exosomes secretion was increased in kidney tissue of CaOx crystal deposition mice and stone patients. **A** Schematic diagram of kidney stone mouse model. **B** BUN, SCr, Ca and oxalate levels in mice. **C**-**D** Representative images of HE, Von Kossa, Tunel staining, F4/80 and KIM-1 (scale bar = 20 μm) and quantitative analysis. **E** mRNA levels of inflammatory chemokines MCP-1, IL-6, TNF-α in control and stone mouse kidneys. **F**-**G** Representative IHC images of CD68 in normal control and stone patients kidneys and quantitative analysis. Scale bar = 20 μm. **H** mRNA levels of macrophage markers CD86, ARG-1 and CD163. **I** Expression levels of genes related to exosome secretion of mice and human. **J**-**K** Protein levels of Rab27a in mouse kidney and human kidney. **L**-**M** Representative IF images and quantitative results of CD63 and TSG101 and proximal RTECs marker AQP-1 in mouse kidney tissues. **N** Representative IHC images and quantitative results of CD63 and TSG101. **O** Representative TEM images showing extracellular vesicles secreted by RTECs at 12d after modelling. Scale bars = 500 nm. **P**-**Q** Representative western blot images and quantitative analysis showed the expression levels of CD63 and TSG101 in the control and CaOx mice, and control and stone patients kidneys. Data are shown as mean ± SEM. P-values were calculated from two-tailed independent t-tests.*$p < 0.05$, **$p < 0.01$, ***$p < 0.001$, ****$p < 0.0001$

patients is significantly increased (Fig. 1F-G). In the kidneys of mice model, mRNA levels of macrophage markers suggested that pro-inflammatory M1 macrophages were the predominant increased (Fig. 1H). These results suggest that CaOx crystal deposition induces significant macrophage infiltration, with a predominance of pro-inflammatory M1 macrophages.

Secretion of extracellular vesicles from kidney proximal tubules was increased in kidney stones mice and patients

To investigate the role of extracellular vesicle (EV) secretion in nephrolithiasis, we examined 3 genes, *Rab27a*, *Rab27b and Smpd3* (Fig. 1I), which are related to extracellular vesicle secretion in mice and human renal tissues [26, 27]. Among these, only *Rab27a* was significantly upregulated (Fig. 1J-K). Immunofluorescence showed that CD63- and TSG101- labelled EVs were mainly localized around proximal renal tubular epithelial cells (Fig. 1L-M). In kidney tissues from nephrolithiasis patients, immunohistochemical (IHC) analysis of CD63 and TSG101 revealed a significant increase in EV secretion compared to controls (Fig. 1N). Transmission electron microscopy (TEM) further confirmed a higher number of EV bodies in the proximal renal tubular epithelial cells of mouse kidneys (Fig. 1O). Western blot results of CD63 and TSG101 in both mouse and human kidney tissues supported the above conclusions (Fig. 1P-Q). These results illustrated that the secretion of extracellular vesicles was increased in the process of nephrolithiasis, suggesting a potential role for EVs in the pathophysiology of kidney stone disease.

CaOx-stimulated exosomes from TCMK-1 cells promoted M1 polarization

TCMK-1 cells were stimulated by 150mmol/ml CaOx, with or without the exosome secretion inhibitor GW4869, for 24 h. The medium was then replaced with exosome-free medium for an additional 24 h. The exosomes in the conditioned medium were collected to stimulate RAW264.7 cells (Fig. 2A). Characterization of exosome markers (CD63, TSG101, CD81 and negative marker Calnexin) by western blot, morphology and size by transmission electron microscopy (TEM) and nanoparticle tracking analysis (NTA) confirmed the successful isolation of control-exosomes (Ctrl-exo) and CaOx-exosomes (CaOx-exo) (Fig. 2B-C). In addition, the concentration of CaOx-exo was significantly higher than Ctrl-exo (Fig. 2D-E), which may be attributed to the increased expression of *Rab27a*. PKH26-labelled exosomes were co-cultured with RAW264.7 cells, confirming that RAW264.7 cells could internalize these exosomes (Fig. 2F). CaOx significantly enhanced exosome secretion from TCMK-1 cells, and macrophages treated with CaOx-exo exhibited a shift toward the pro-inflammatory M1 phenotype. In contrast, macrophages treated with exosomes derived from TCMK-1 cells exposed to both GW4869 and CaOx showed reduced M1 polarization (Fig. 2G-I, Fig S1A).

To further clarify the relationship between exosomes and kidney inflammation in vivo, we constructed *Rab27a* knockout mice (Rab27a-/-) (Fig. S1B-C). As expected, the kidney of Rab27a-/- mice exhibited less M1 polarization compared to than wild-type mice (Fig. 2J, Fig S1D). Flow cytometry further demonstrated that CaOx-exo promoted a pro-inflammatory M1 phenotype, while GW4869 mitigated this effect (Fig. 2K). In CaOx-exo-treated macrophages, mRNA levels of M1 markers (TNF-α, iNOS, CD86) were significantly upregulated, while M2 markers (CD163, IL-10, TGF-β1, Arg-1) were downregulated (Fig. 2L). RAW264.7 exposed to CaOx-exo secreted higher levels of proinflammatory cytokines, such as IL-6, IL-8 and TNF-α, and lower levels of anti-inflammatory IL-10, compared to Ctrl-exo-treated cells (Fig. 2M). The above findings suggested that CaOx-exo derived from TCMK-1 induced M1 polarization, contributing to a pro-inflammatory environment.

Exosomal mir-93-3p targeting macrophage NFAT5 May be a potential mechanism of kidney injury induced by stones

MiRNAs sequencing of Ctrl-exo and CaOx-exo revealed 57 significantly up-regulated and 46 significantly down-regulated miRNAs ($|\log2FC|>2.5$, $P<0.01$) (Fig. 3A). After filtering out low-expression miRNAs and screening for homologous ones, we narrowed the candidates to 15 miRNAs (Fig. 3B). By intersecting the above 15 candidates with the differentially expressed miRNAs of folic acid-induced kidney injury and fibrosis (GSE61382), and unilateral ureteral obstruction (UUO) (GSE118340), we

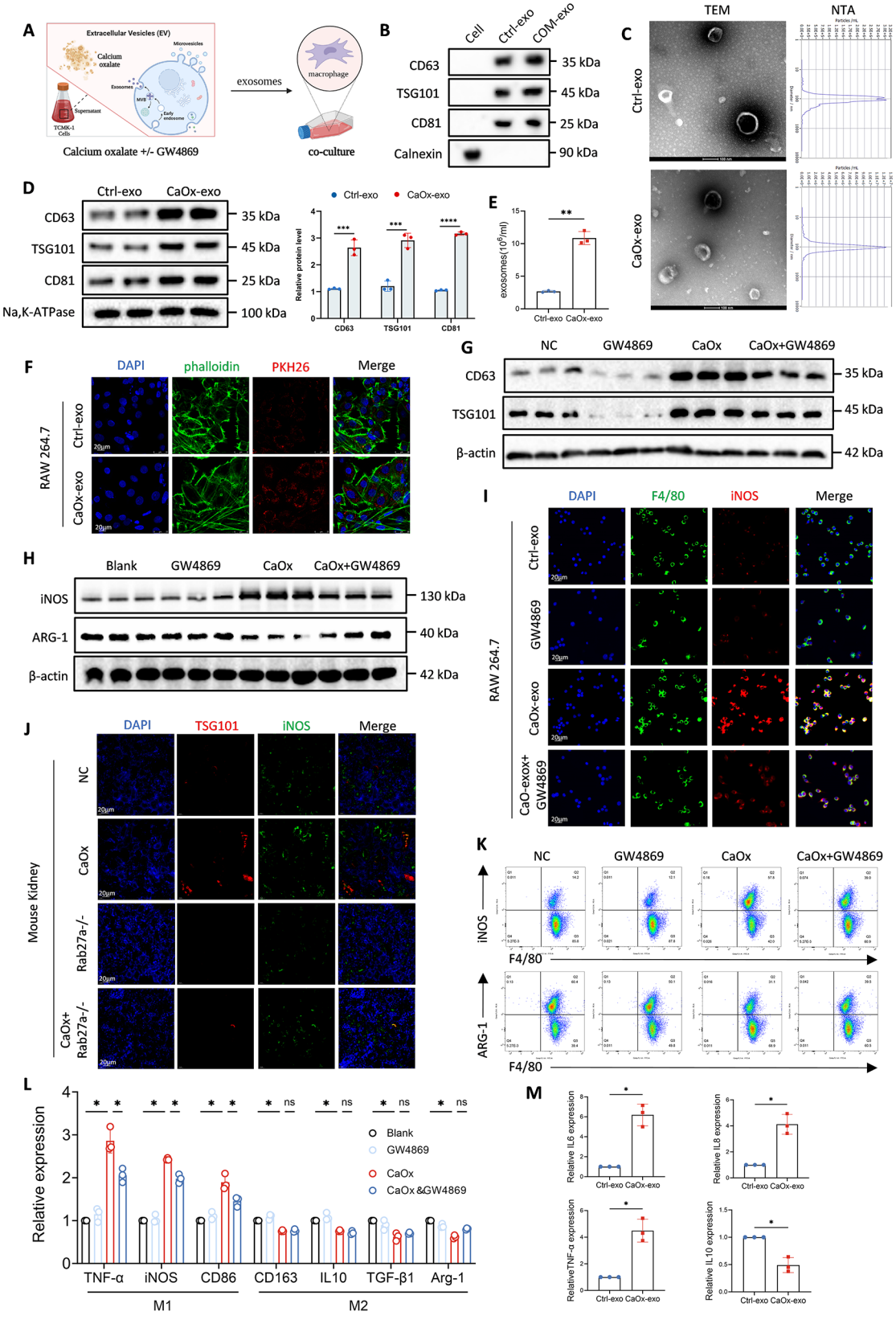

Fig. 2 (See legend on next page.)

(See figure on previous page.)

Fig. 2 CaOx-stimulated exosomes from TCMK-1 promoted M1 polarization. **A** Schematic representation of macrophages treated with exosomes derived from TCMK-1 cells. **B** Exosomes were identified by surface markers. **C** TEM and NTA images of exosomes from TCMK-1 cells. Scale bars = 100 nm. **D** Exosome concentration was assessed by western blot analysis of the same volume of Ctrl-exo and CaOx-exo. **E** Density detection of Ctrl-exo and CaOx-exo. **F** Representative IF image of TCMK-1 cell-derived exosomes taken up by RAW264.7 cells (green for phalloidin and red for PKH- labelled exosomes). Scale bars = 20 μm. **G** Representative western blot of CD63 and TSG101 in TCMK-1 treated with GW4869 and CaOx. **H** Representative western blot of iNOS and ARG-1 in RAW264.7 treated with exosomes from **G** groups. **I** Representative IF images of M1 macrophage markers F4/80 and iNOS in four groups of macrophages. **J** Representative IF images showing the levels of TSG101 and iNOS in the kidneys of stone-induced control and Rab27a-/- mice. **K** Representative flow cytometry results showed four groups of iNOS + F4/80 + and ARG-1 + F4/80 + macrophages, which represent changes in M1 and M2 levels. **L** Relative mRNA levels of representative markers of M1 and M2 macrophages, M1 markers were significantly changed by CaOx stimulation and GW4869. **M** Cytokines produced by Ctrl-exo and CaOx-exo-treated macrophages were assayed by ELISA. Data are shown as mean ± SEM. In D, E, M, p-values were calculated from two-tailed independent t-tests. *$p < 0.05$, **$p < 0.01$, ***$p < 0.001$, ****$p < 0.0001$

identified two potential targets: mmu-miR-27-5p and mmu-miR-93-3p (Fig. 3C). RNA sequencing of macrophages treated with exosomes revealed enrichment of inflammatory pathways and pro-inflammatory factor production based on KEGG and GO analyses (Fig. 3D, Fig S2A). To pinpoint the key pro-inflammatory miRNA, TCMK-1 cells were transfected with miR-27-5p or miR-93-3p mimics or inhibitors, and the polarization of macrophages was assessed. Transfection of mimics of miR-93-3p but not miR-27a-5p resulted in a significant increase of iNOS expression, indicating that the former was the primary contributor to M1 polarization (Fig. 3E-F, Fig S2B-C). After filtering, we identified NFAT5 as the potential target gene of miR-93-3p using 5 miRNA target gene prediction tools (TargetScan, miRDB, miRWalk, miRmap and Tarbase) (Fig. 3G). Nuclear factor of activated T-cells 5 (NFAT5) is known to play a key role in inflammation and immune responses triggered by damage-associated molecular patterns (DAMPs). Notably, previous studies have shown that NFAT5 contributes to the progression of chronic arthritis by promoting macrophage polarization [28]. RT-qPCR analysis confirmed that NFAT5 expression was reduced in macrophages treated with CaOx-exo (Fig. 3H). Bioinformatics analysis revealed a complementary binding sequence between miR-93-3p and the 3′ untranslated region (3′UTR) of NFAT5 (Fig. 3I). Cells co-transfected with miR-93-3p mimics and a luciferase reporter plasmid containing WT NAFT5 3'UTR showed lower luciferase activity (Fig. 3J). IHC and Western blot analyses showed that NFAT5 expression was significantly lower in the kidney tissues of CaOx mice and nephrolithiasis patients than in controls (Fig. 3K-L, Fig S2D). Based on these findings, we selected miR-93-3p for further research and concluded that CaOx-exo regulates renal injury caused by kidney stones through exosomal-miR-93-3p/NFAT5 axis.

The NIK/NF-κB2 pathway promotes M1 polarization and METs formation

The NIK/NF-κB2 pathway in the RNA sequencing results of macrophages emerged as a key area of interest (Fig. 3D). Analysis from the public database (humphreyslab.com/SingleCell/) revealed that significantly increased expression NIK(Map3k14) in the kidneys of mice 14 days after UUO surgery. NIK is mainly expressed in macrophages and repairing renal tubular epithelial cells (Fig S3) [29]. To further verify the regulatory effect of miR-93-3p on NFAT5 and NIK/NF-κB2 pathway, Western blot was performed to assess the levels of the key molecules in RAW264.7 cells. Not surprisingly, NIK and its downstream p52 were significantly increased, while p100, the precursor of p52, and NFAT5 were decreased when cells were stimulated with CaOx-exo and transfected with miR-93-3p mimics. Conversely, when cells were treated with CaOx-exo and transfected with miR-93-3p inhibitors, NIK and p52 levels increased significantly. Co-transfection with LV-NFAT5 further amplified these changes (Fig. 4A-B). Additionally, treatment with miR-93-3p inhibitor and/or si-NIK reduced p100 levels while increased p52 levels compared to the control group (Fig. 4C-D). These findings suggest that miR-93-3p and NIK both act as key regulators in suppressing the NF-κB2 pathway.

In addition to regulating inflammatory factors and pro-inflammatory pathways, we found the term "extracellular space" in the results of KEGG enrichment analysis (Fig. 3D). Recent studies reported a novel form of macrophage death, known as METosis, characterized by the release of DNA and proteins into the extracellular space to form structures called METs. To confirm the presence of METs, we stained extracellular DNA meshwork structures along with MET markers (citH3 and MMP12). Consistent with the previous results, IF results showed that CaOx-exo-stimulated macrophages were polarized into M1 phenotype, and METs formation was significantly increased, which could be reversed by using miR-93-3p inhibitor and si-NIK (Fig. 4E-F). In summary, CaOx-exo exacerbated inflammation and kidney injury induced by kidney stones by promoting M1 polarization and METs release.

NFAT5 repressed NIK/NF-κB2 pathway via ubiquitination and degradation of NIK by Akt1/cIAP1/2

We used the STRING database to identify the mediator molecule between NFAT5 and NIK/NF-κB2. 10 molecules were related with NFAT5, and among them, only

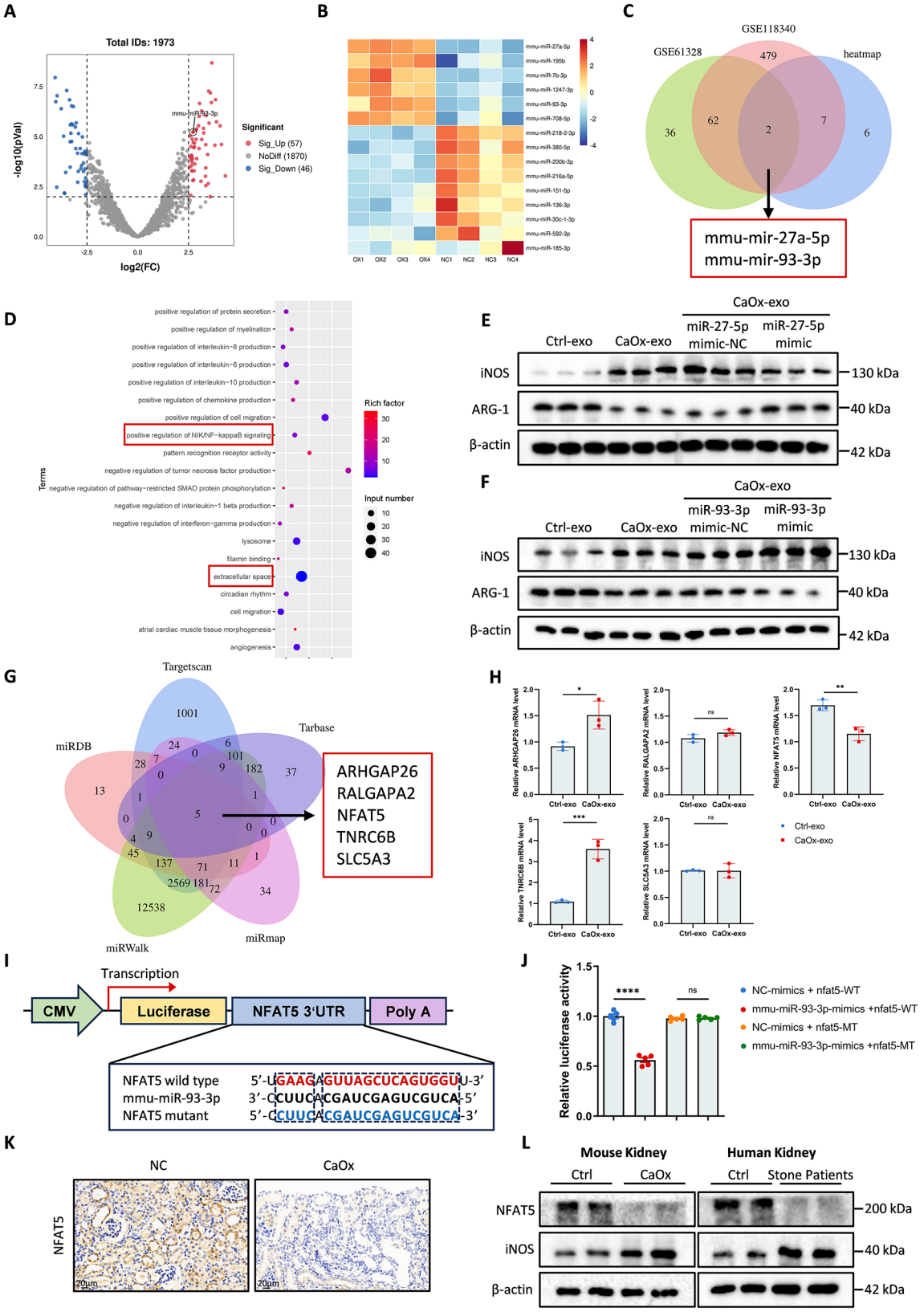

Fig. 3 (See legend on next page.)

(See figure on previous page.)

Fig. 3 Exosomal mir-93-3p targeting macrophage NFAT5 may be a potential mechanism of kidney injury induced by stones. **A** Volcano plot of miRNA sequencing. **B** Heat map of miRNA sequencing. **C** 2 candidate miRNAs were obtained after intersection of genes in the heat map with GSE61328 and GSE118340. **D** KEGG enrichment analyses were performed on the RNA sequencing results of CaOx-exo and Ctrl-exo-treated macrophages. **E** The mimics and inhibitors of miR-27a-5p and miR-93-3p were used to verify their effects on macrophage polarization, respectively. **G** Venn diagram showing the intersection of potential target genes of miR-93-3p predicted by 5 databases: TargetScan, miRDB, Tarbase, miRWalkand miRmap. **H** Relative mRNA levels of the 5 genes in the intersection. **I** The binding site of wild-type NAFT5 with miR-93-3p, and mutant sequence of NFAT5 3′-UTR. **J** Luciferase activity of cells cotransfected with mimics-NC or miR-93-3p mimics and NFAT5-WT or NFAT5-Mut luciferase reporter plasmid. **K** Representative IHC images indicating NFAT5 expression levels in mouse kidneys. Scale bars = 20 μm. **L** The expression levels of NFAT5 and iNOS in mouse and human kidney tissues were detected by Western blot. Data are shown as mean ± SEM. In H, P-values were calculated from two-tailed independent t-tests. In J, One-way ANOVA with Tukey's multiple comparisons test. *$p < 0.05$, **$p < 0.01$, ***$p < 0.001$, ****$p < 0.0001$

Akt1 was part of the of NF-κB2 signalling pathway cluster (Fig. 5A). Therefore, we hypothesized that NFAT5 regulates the NIK/NF-κB2 pathway through Akt1. Western blot analysis revealed that knocking down NFAT5 reduced the levels of p-Akt1/Akt1 and cIAP1/2 while increasing NIK levels (Fig. 5B). si-NFAT5 potentiated the CaOx-exo-induced increase in NIK expression (Fig. 5C). In RAW264.7 cells, Akt1 phosphorylation was inversely correlated with NIK protein levels in a dose-dependent manner (Fig S4A). Given Cycloheximide (CHX) to cells to inhibit protein synthesis, treatment with the Akt1 activator SC79 promotes NIK degradation, whereas NIK exhibited an extended half-life in the absence of SC79 (Fig S4B). Ubiquitination is a common post-translational modification (PTM) involved in protein degradation, and previous studies have identified cIAP1/2 as the primary E3 ubiquitin ligases targeting NIK for degradation [30, 31]. The public PTM database further confirmed the presence of multiple ubiquitination and phosphorylation sites on NIK (Fig S4C). To examine the roles of NFAT5 and Akt1 affect NIK ubiquitination and degradation, cells were treated with NFAT5 or cIAP1/2 overexpression plasmids, SC79, or proteasome inhibitor MG132, respectively. Overexpression of NFAT5 or cIAP1/2, or treatment with SC79 reduced NIK protein levels, whereas MG132 co-treatment inhibited NIK degradation (Fig. 5D). We further examined the levels of ubiquitination in RAW264.7 in different conditions. Co-immunoprecipitation experiments showed that NFAT5 promoted NIK ubiquitination (Fig. 5E). Activation of Akt1 by SC79, or overexpression of cIAP1/2 also promoted NIK ubiquitination (Fig. 5F-G). These results demonstrate that NIK degradation mediated by p-Akt1 is associated with NIK ubiquitination. NFAT5 promotes Akt1 phosphorylation, which activates cIAP1/2. These E3 ubiquitin ligases directly ubiquitinate NIK, thereby suppressing the NF-κB2 pathway.

Considering that Akt1 is a canonical kinase and NIK has some phosphorylation modification sites, we performed CO-IP and found no direct interaction between NIK and p-Akt1 (Fig S4D). In RAW264.7 cells overexpressing NIK or treated with SC79, p-Akt1 increased p52 protein level, without altering NIK phosphorylation (Fig S4E). This may be linked to IKKα activation, another critical kinase in the NF-κB2 pathway, mediated by Akt1.

Overall, our results indicate that p-Akt1 promotes cIAP1/2 expression, which in turn ubiquitinates and degrades NIK. NFAT5, acting as an upstream regulator of Akt1, allows NIK to escape from ubiquitination-mediated degradation when down-regulated by exosomal-miR-93-3p, thereby inhibiting the NF-κB2 pathway.

Tubular epithelial cells derived miR-93-3p promotes M1 polarization and METs formation in vivo

To investigate the correlation between proximal tubular epithelia cells derived exosomes and CaOx-induced renal inflammation, we performed an animal study in a CaOx mice model by tail intravenous injection of CaOx-exo or Ctrl-exo (Fig. 6A). CaOx-exo injection significantly exacerbated renal dysfunction compared to Ctrl-exo-treated normal control (NC) and CaOx mice (Fig. 6B). TCMK-1-derived exosomes were labelled with DiR, and their biodistribution was tracked through fluorescence imaging of the lungs, liver, and kidneys at 6, 12, 24, and 48 h post-injection. Fluorescence intensity increased over time, with the highest accumulation in the lungs, followed by the liver, and comparatively lower levels in the kidneys at all time points (Fig S5A). After accounting for fluorescence interference from other organs, kidney uptake of exosomes was observed to increase over time, peaking at 48 h (Fig S5B). Based on these findings, subsequent in vivo experiments focused on the fluorescence intensity at the 48-hour time point.

Interestingly, CaOx-exo injection in CaOx mice resulted in significantly higher exosome uptake in the kidneys compared to Ctrl-exo-treated NC mice (Fig. 6C). This suggests that CaOx-exo exacerbates pre-existing renal injury caused by kidney stones, potentially through enhanced macrophage phagocytosis or upregulated expression of scavenger receptors, thereby increasing the uptake of exogenous exosomes [32]. In addition, NFAT5 specifically overexpressed stone mice and miR-93-3p antagomir intravenously injection stone mice models were established. M1 polarization, METs formation, and NIK/NF-KB2 pathway were attenuated by NFAT5 overexpression or antagomir (Fig. 6D-E). Histological analyses using HE and Von Kossa staining demonstrated

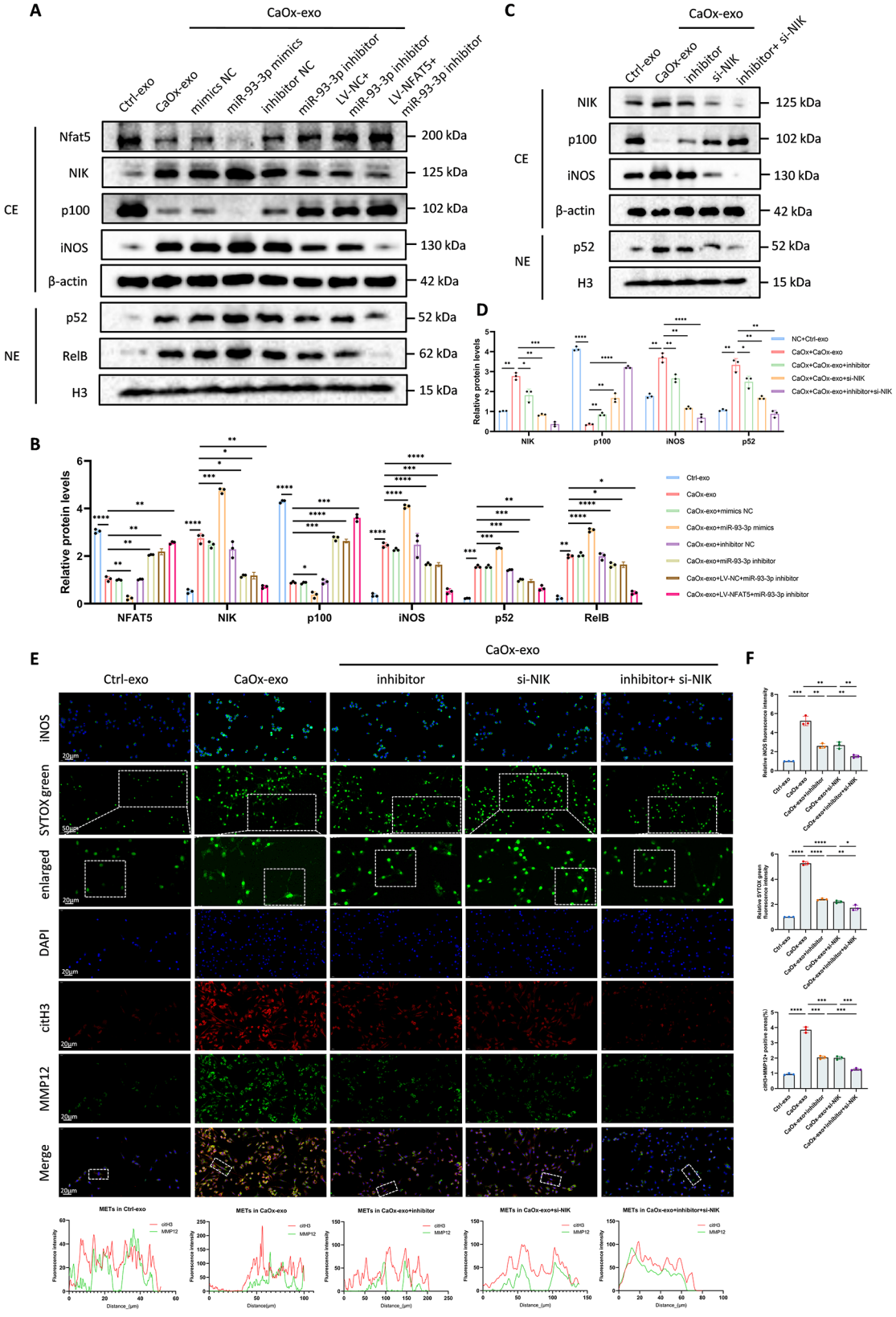

Fig. 4 The NIK/NF-κB2 pathway promotes M1 polarization and METs formation. **A**-**B** Representative western blot results showed the levels of NFAT5, NIK, p100, p52 and RelB in RAW264.7 cells stimulated with different groups of TCMK-1-derived exosomes. **C**-**D** Western blot analysis of NIK, iNOS, p100 and p52 when NIK is knocked down. **E**-**F** SYTXO-green staining showed the formation of METs, and citH3 + MMP12 + RAW264.7 represented cells undergoing METosis. Data are shown as mean ± SEM. Two-way ANOVA with Tukey's multiple comparisons test.*$p < 0.05$, **$p < 0.01$, ***$p < 0.001$, ****$p < 0.0001$

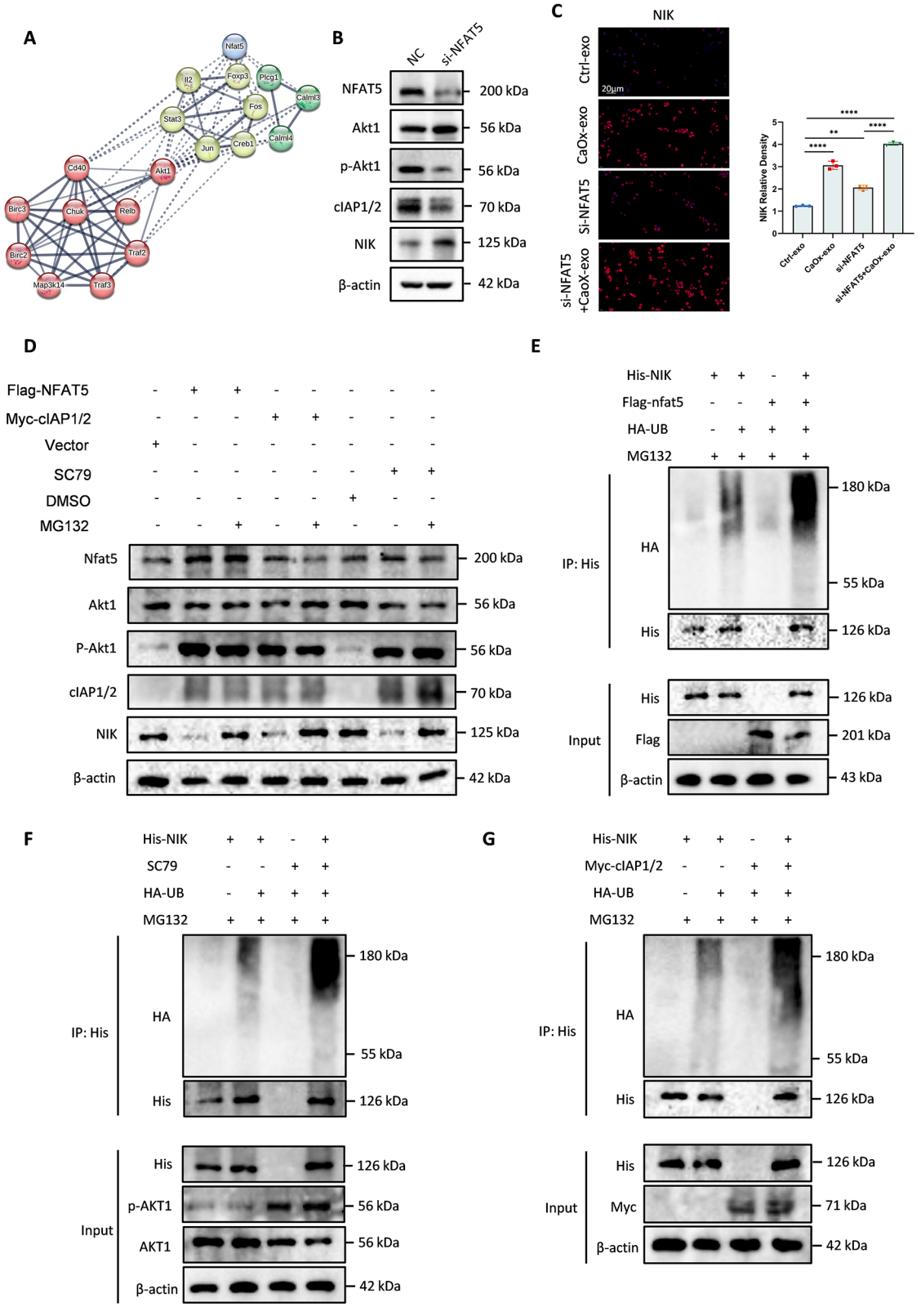

Fig. 5 (See legend on next page.)

(See figure on previous page.)

Fig. 5 NFAT5 repressed NIK/NF-κB2 pathway via ubiquitination and degradation of NIK by Akt1/cIAP1/2. **A** Protein-protein interaction networks for NFAT5 and NIK/ NF-κB2 pathway were constructed using the STRING online database. **B** Protein levels of NFAT5, Akt1,p-Akt1, cIAP1/2 and NIK in macrophages transfected with NC or si-NAFT5 were determined using Western blot. **C** Representative images and quantitative analysis of IF staining of NFAT5 in RAW264.7 cells in 4 different treatment groups. Scale bar = 20 μm. **D** Protein levels of NFAT5, Akt1,p-Akt1, cIAP1/2 and NIK in macrophages transfected with Flag-NFAT5, Myc-cIAP1/2 plasmids or applied with SC79, DMSO or MG132, were determined using Western blot. **E**–**G** TCMK-1 cells were transfected with different plasmids and treated with MG132. Cell lysates were immunoprecipitated with Myc antibody. Ubiquitinated and total NIK was detected by immunoblot analysis of anti-HA and anti-FLAG antibodies. Immunoblot analysis of NFAT5, Myc (NIK), HA (Ub), and β-actin in whole-cell lysates. Data are shown as mean ± SEM. Two-way ANOVA with Tukey's multiple comparisons test.*$p < 0.05$, **$p < 0.01$, ***$p < 0.001$, ****$p < 0.0001$.

reduced kidney injury and stone formation following NFAT5 overexpression or miR-93-3p inhibition. AAV-NFAT5 or antagomir decreased NIK expression and increased NFAT5 and p-AKT1 levels, and METs co-labelled with citH3, the marker of METs, and F4/80 can also be suppressed (Fig. 6F-G). These results revealed that exosomal miR-93-3p modulates the NFAT5/AKT1/NIK/NF-κB2 axis in vivo, contributing to renal inflammation and injury associated with kidney stones.

METs and M1 polarization formed a positive feedback loop in kidney injury

To further elucidate the critical role of NIK/NF-κB2 and METs in CaOx-exo-induced kidney injury, we used METs inhibitor CI-amidine or NIK inhibitor NIK SMI1 to suppress METs production and NIK/NF-κB2 pathway in mice, respectively. As expected, both treatments attenuated pathological changes, including renal tubule lumen dilation, crystals deposition, M1 polarization, and the presence of citH3 and F4/80-labeled METs (Fig. 7A-B). Western blot analysis confirmed the reduced expression of iNOS and citH3 proteins in the kidney tissues of treated mice, aligning with staining results (Fig. 7C-D). Furthermore, ionomycin, an activator of extracellular traps, significantly increased METs formation, as well as the co-localization of citH3 and MMP12 in macrophages. It also enhanced M1 polarization in murine bone marrow-derived macrophages. However, both CI-amidine and NIK SMI1 effectively mitigated these effects (Fig. 7E-F). In each group of macrophages, we evaluated the expression levels of citH3 and iNOS. Western blot analysis confirmed that both inhibitors effectively inhibited the upregulation of citH3 and iNOS, as well as M1 polarization by CaOx and Ionomycin (Fig. 7G-H). In conclusion, pro-inflammatory macrophages and their distinct modes of cell death mutually amplify each other, creating a positive feedback loop that exacerbates kidney injury.

miR-93-3p is specifically down-regulated in TCMK-1 cells by the master transcription factor complex CREB1/CRTC2

To explore the mechanism of by which CaOx stimulated the increased expression of miR-93-3p in TCMK-1 cells, we searched the specific transcription factors of mmu-miR-93-3p in the public online database TransmiR (v3.0,cuilab.cn/transmir). Screening for transcription factors with Level 1 evidence specifically expressed in the kidney, we found that CRTC2 is highly kidney-specific (Table S1). CREB1, a coactivator of CRTC2, was also identified as a candidate. Therefore, we focused on the regulation of miR-93-3p by CREB1/CRTC2 complex. Intraperitoneal injection of $1,25(OH)_2D_3$ is commonly used to establish nephrolithiasis models in mice [33]. Analysis of ChIP-seq data from GSE206777 revealed that both p-CREB1 and CRTC2 were enriched upstream of the miR-93 host gene (miR-93 HG) promoter, with CRTC2 showing significant enrichment under $1,25(OH)_2D_3$ stimulation (Fig. 8A). This suggests that the transcription coactivator CRTC2 may be the main factor responsible for the increased miR-93-3p expression. CHIP assay showed that CRTC2, but not p-CREB1, regulated miR-93-3p expression after CaOx stimulation in TCMK-1 cells (Fig. 8B-C). Electrophoretic mobility shift assay (EMSA) was performed to further demonstrate the specific binding region of CREB1/CRTC2 to the miR-93 HG promoter. Binding to the miR-93 HG promoter was observed only in protein extracts from cells stably expressing CREB1 but not with extracts from cells stably expressing CRTC2, and specificity was confirmed by the reduced binding in the presence of competitive probes (Fig. 8D). This is consistent with the typical structure and function of the CREB1/CRTC2 complex. Therefore, we hypothesized that CREB1 directly binds to the promoter of miR-93 HG, but its enrichment remains constant regardless of stimulation. In contrast, CRTC2 binds indirectly to the promoter region via CREB1, and is significantly enriched during stimulation, functioning as the dominant transcription factor (Fig. 8G). TransmiR provided the putative motif logo for CREB1, highlighting two potential binding sites on the promoter region (Fig. 8E). CHIP-qPCR revealed that the binding site 1(-243 to -238 bp) was responsible for CREB1/CRTC2-mediated miR-93 HG promoter activity (Fig. 8F). Luciferase reporter assays in 293T cells showed that transfection of CREB1 or CRTC2 plasmids significantly increased promoter activity, with CRTC2 demonstrating a stronger effect. However, the transcriptional effect of CREB1 or CRTC2 on mutant miR-93 HG was significantly reduced. For miR-93 HG + CRTC2 + shCREB1 group, the luciferase activity was not only lower than that of miR-93 HG + CREB1 + shCRTC2 group but also more significantly lower than that of mir-93 HG + CRTC2 group (Fig. 8H). These results revealed that CREB1/

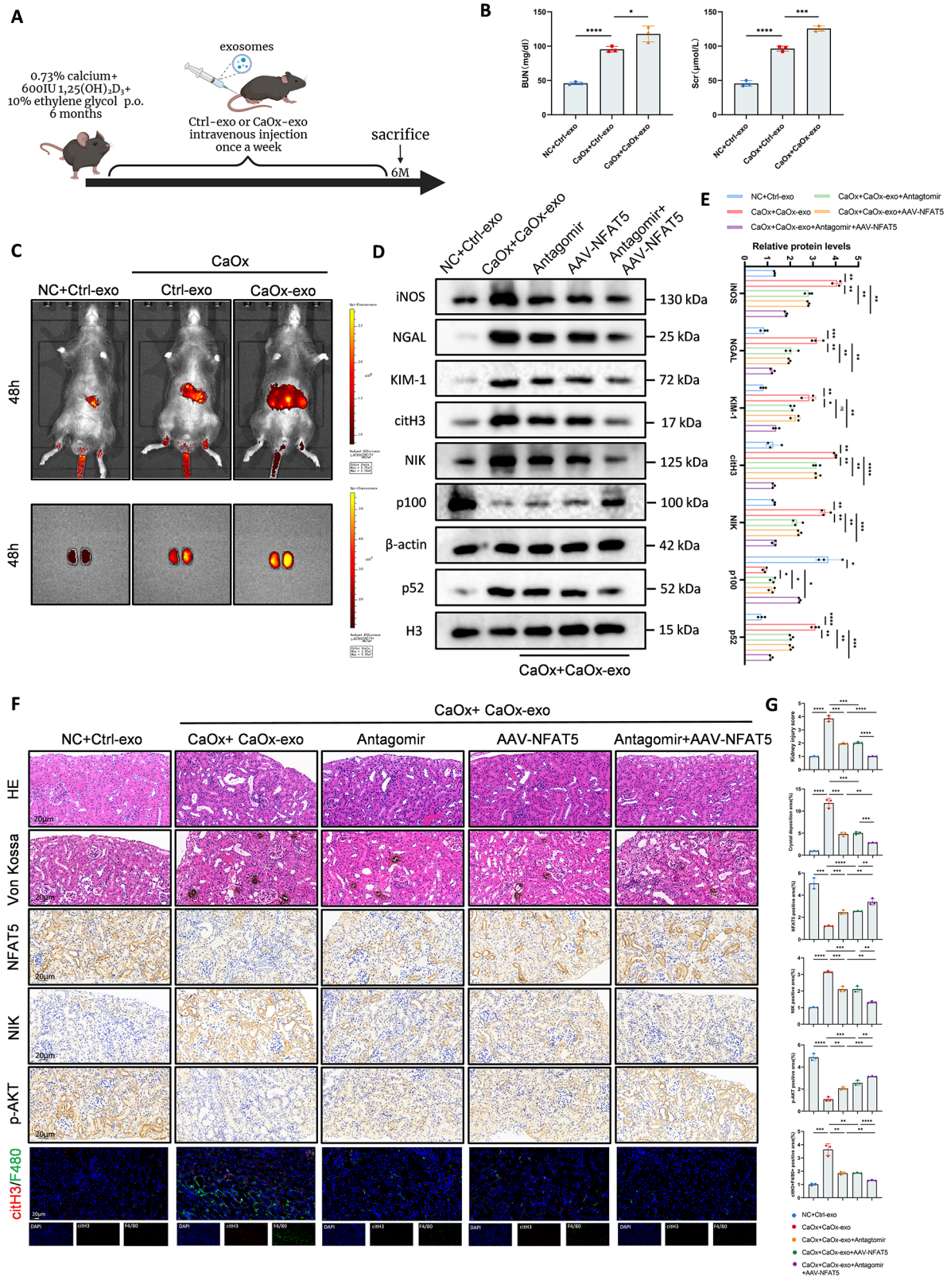

Fig. 6 (See legend on next page.)

(See figure on previous page.)

Fig. 6 Tubular epithelial cells derived miR-93-3p promotes M1 polarization and METs formation in vivo. **A** Schematic diagram of the kidney stone mouse model by tail intravenous injection exosomes. **B** Renal function in each group of mice. **C** DIR-labelled exosomes were observed in vivo to evaluate exosome uptake efficiency by the kidneys after modelling. **D**-**E** Protein levels of iNOS, NGAL, KIM-1, citH3, NIK, p100 and p52 in kidneys of different groups. **F**-**G** Representative pathological staining images, IHC images and IF images showing the expression of kidney injury, crystal deposition, NFAT5, NIK, p-AKT and citH3 + F4/80 + areas. Scale bar = 20 μm. Data are shown as mean ± SEM. Two-way ANOVA with Tukey's multiple comparisons test.*$p < 0.05$, **$p < 0.01$, ***$p < 0.001$, ****$p < 0.0001$

CRTC2 is a specific transcriptional activator complex of miR-93 HG. While CREB1 is essential for transcription activation, CRTC2 plays a predominant role in enhancing transcription.

Discussion

The formation of kidney calculi is mainly related with the deposition and growth of supersaturated crystals in the urine [34]. The stimulated RTECs engage in crosstalk with a variety of other cells in the environment, such as macrophages and fibroblasts, resulting in cascade amplification of inflammatory injury and increased formation of extracellular matrix [35]. Among them, the communications between RTECs and macrophages is essential for crystal clearance and inflammatory modulation. Multiple studies have found that ischemic/hypoxic stimulation enhances macrophage-derived exosome production, exacerbating RTEC damage [36]. While macrophages can sense urinary constituents via transepithelial protrusions to phagocytize crystals and prevent tubular obstruction [37], current understanding remains incomplete regarding epithelial-derived exosomal mechanisms in macrophage-mediated renal injury [23]. It is primarily M2 that performs the functions of crystal clearance and tissue repair [38, 39], whereas M1 macrophages promote crystal aggregation and inflammatory responses [40]. This study specifically investigates the molecular pathways through which RTEC-derived exosomes drive M1 macrophage polarization.

Exosomes are microvesicles with lipid membranes, which can transport bioactive cargo (proteins, lipids and nucleic acids) into recipient cells to participate in intercellular communication [41]. Rab GTPases, (particularly Rab27a/b), critically regulate exosomal biogenesis and secretion [42]. In this study, our team constructed Rab27a knockout (Rab27a-/-) mice to reduce exosome secretion [43]. Rab27a-/- mice exhibited attenuated nephrolithiasis severity and reduced crystal deposition, establishing a pathological link between RTEC-derived exosomes and stone formation. This aligns with prior observations of oxalate-induced exosome overproduction in lithogenesis [44]. Tail intravenous injection of CaOx-exo into kidney stone mice resulted in more severe kidney injury than Ctrl-exo. This differential effect stems from both compositional alterations in CaOx-exo cargo and inflammation-enhanced exosomal release/uptake dynamics.

MicroRNAs(miRNAs) constitute critical regulators in the renal calculi formation and subsequent kidney injury, with emerging potential as diagnostic biomarkers [45]. In this study, we explored the packaged differentially expressed miRNAs in Ctrl-Exo and CaOx-Exo by miRNA sequencing, and miR-93-3p was significantly highly expressed in CaOx-exo with homology. Previous studies have linked miR-93-3p to various pathological processes. For instance, miR-93-3p expression is elevated after severe burns in mice, promoting intestinal mucosal injury and inhibiting tissue repair [47]. In addition, a significant increase in miR-93-3p expression was identified in renal clear cell carcinoma, and the potential activated signalling loop STAT3-miR-93-3p-DAPK1 could exacerbate cancer progression [48]. ASMTL-AS1, a down-regulated lncRNA in papillary thyroid carcinoma, increased the expression of miR-93-3p, which promoted glycolysis and tumor development [49]. However, its involvement in CaOx nephropathy remains uncharacterized. In the present study, we found that RTECs-derived exosomal miR-93-3p drives M1 macrophage polarization, thereby initiating inflammatory cascades that potentiate renal injury.

By integrating macrophage RNA sequencing, bioinformatics analysis and qRT-PCR validation, we identified NFAT5 as a direct target of miR-93-3p. Macrophages exposed to CaOx-exo exhibited NFAT5 downregulation concomitant with upregulated pro-inflammatory pathways (cytokine secretion, extracellular matrix remodeling). NFAT5 was originally identified as a transcriptional regulator of hypertonic salt stress responses in the renal medulla. It was later confirmed to be implicated in inflammation and oxidative stress [50]. For example, NFAT5 activates mTOR-IRF3/7 to exacerbate kidney injury in patients and mouse models of lupus nephritis [51], and its interaction with NF-κB enhances glycolysis and inflammatory responses in macrophages during sepsis [52]. The present study demonstrated that, consistent with its anti-inflammatory potential, NFAT5 overexpression attenuated CaOx-exo-induced crystal deposition and renal pathology. We also found that CaOx-exo-accelerated macrophage polarization and inflammation is miR-93-3p/NFAT5 axis dependent for the first time.

The link between kidney stones and inflammation has garnered increasing attention [4, 53]. According to Yang et al., macrophage polarization status is closely related to crystal burden and renal pathology [36]. However,

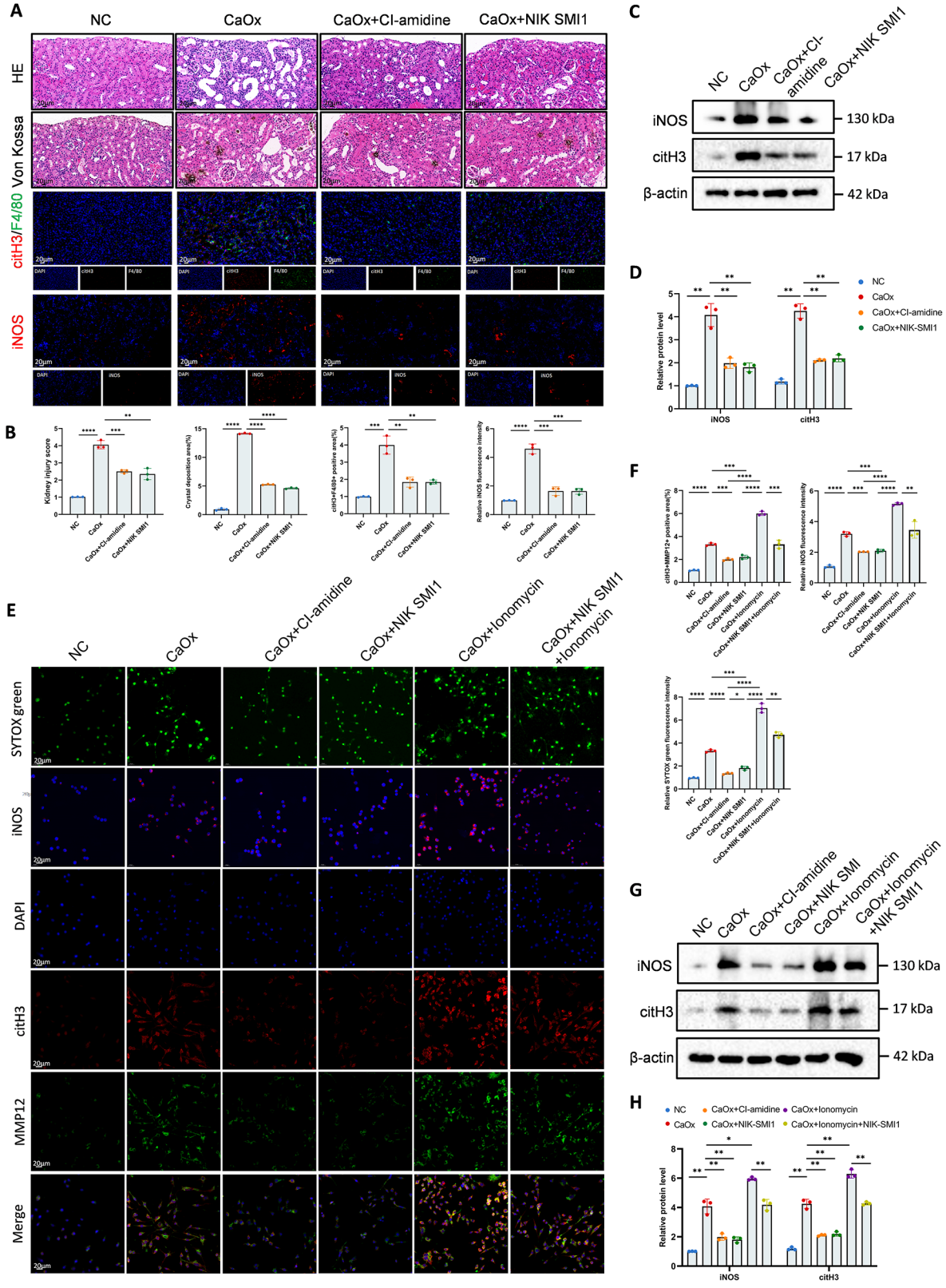

Fig. 7 (See legend on next page.)

(See figure on previous page.)

Fig. 7 METs and M1 polarization formed a positive feedback loop in kidney injury. **A**-**B** Representative images and quantitative analysis HE, Von Kosaa, and IF images showing the expression of iNOS+, and citH3 + F4/80 + areas. Scale bar = 20 μm. **C**-**D** Western blot bands and quantitative protein expression levels of iNOS and citH3 in kidney tissues from 4 groups of mice. **E**-**F** citH3 + F4/80+, iNOS + cells and METs formation were detected by IF after pretreatment of BMDMs with Cl-amidine, NIK SMI1, or Ionomycin. The results were quantified. Scale bar = 20 μm. **G**-**H** Western blot bands and quantitative protein expression levels of iNOS and citH3 in BMDMs in 6 groups. Data are shown as mean ± SEM. Two-way ANOVA with Tukey's multiple comparisons test.*$p < 0.05$, **$p < 0.01$, ***$p < 0.001$, ****$p < 0.0001$.

the mechanisms by which CaOx-exo and miR-93-3p/NFAT5 axis regulate inflammation have not been elucidated. KEGG pathway enrichment analysis showed that NFAT5 may participate in the regulation of macrophage inflammatory response through NIK/ NF-κB2 signaling—a non-canonical pathway involving p100 precursor processing into transcriptionally active p52/RelB dimers that mediate immune regulation and inflammation [54–56]. Our data suggest that NFAT5 silencing activates NIK/ NF-κB2 pathway through enhanced NIK stability. Interestingly, NFAT5 could promote NIK ubiquitination via cIAP1/2 E3 ligases, regardless of CaOx-exo presence [57, 58]. Akt1 was identified as an upstream kinase that activates cIAP1/2 and promotes apoptosis in human leukemic cells [59]. Results from the STRING database showed a potential association between NFAT5 and Akt1, leading us to hypothesize that CaOx-exo, as an external stimulus, inhibits Akt1/cIAP-mediated NIK degradation, thereby activating NF-κB2 signaling and accelerating kidney injury. Briefly, in CaOx-exo-induced macrophages, CREB1/CRTC2 promotes the expression of miR-93-3p, which directly targeted NFAT5. The inhibition of the Akt1/cIAP1/2 pathway reduces NIK ubiquitination, thereby activating the NIK/NF-κB2 pathway up-regulated the expression of downstream pro-inflammatory and immunomodulatory genes. The interplay between pro-inflammatory M1 macrophages and METs creates a positive feedback loop that exacerbates kidney injury (Fig. 9).

However, our study focused on miR-93-3p and its downstream pathways, it remains unclear whether other exosomal cargo (lncRNAs, mRNAs, scaffold proteins) warrant systematic exploration. Actually, in addition to delivering miRNAs, more and more nanobiotechnology, with its unique nanoscale precision, targeted delivery and multifunctional integration, has opened up a new path for the precise diagnosis and treatment of kidney stones and kidney injury [60]. For example, surface-engineered nanoparticles enable lesion-specific release of stone-modulating agents (e.g., potassium citrate, Tamm-Horsfall protein) while minimizing systemic toxicity [61]. In addition, nanobiotechnology can be used for stone composition analysis and dynamic monitoring of kidney injury. Development of surface-enhanced Raman scattering (SERS)-based nanoprobes permit non-invasive stone composition analysis via metabolite spectral fingerprints [62]. Glutathione-functionalized gold nanoparticles (GS-AuNPs) coupled with photoacoustic imaging enable real-time glomerular filtration rate (GFR) monitoring for acute kidney injury detection [63]. Finally, ceria-based nanocomposites simultaneously scavenge ROS, preserve mitochondrial integrity, and mitigate tubular damage, demonstrating synergistic intervention from stone formation [64].

Our study contributes to a deeper understanding of the mechanism of CaOx-induced M1 polarization, by concentrating on the specific miRNA and pathway. Regulation of macrophage polarization by epithelial-derived exosomes, and treatment with functional nanomaterials offer a promising avenue for kidney stone therapy. In brief, the present study lays a solid foundation for understanding the pathogenesis of CaOx-induced kidney injury and identifies potential therapeutic targets for clinical intervention.

Methods

Human studies

Patients at Renmin Hospital of Wuhan University with severe hydronephrosis due to kidney stones underwent nephrectomy, the obtained nonfunctioning kidneys were divided into the "stone patients" group ($n = 6$). The adjacent to cancer tissues of 6 patients who underwent radical nephrectomy were selected as controls. All participants provided informed consent, and ethical approval was acquired from the Ethics Committee of the Renmin Hospital of Wuhan University (WDRY2021-KS047).

Animals

Male C57BL/6 mice, weighing 20–25 g, were purchased from Laboratory Animal Welfare andEthics Committee of Renmin Hospital of Wuhan University (Hubei, China); male Rab27a knockout (Rab27a-/-) mice weighing 20–25 g were purchased from Cyagen Biotechnology, China. All treatments of animals were approved by the Animal Welfare and Ethics Committee of the People's Hospital of Wuhan University (approval number: WDRM20200604).

The mice were given free access to food containing 0.73% calcium and 600IU $1,25(OH)_2D_3$ and drinking water containing 10% ethylene glycol for a period of 6 months to established the CaOx stone model. Mice were randomly divided into control group and CaOx group (each group $n = 6$). After 6 months, mice were euthanized, kidneys and serum were collected.

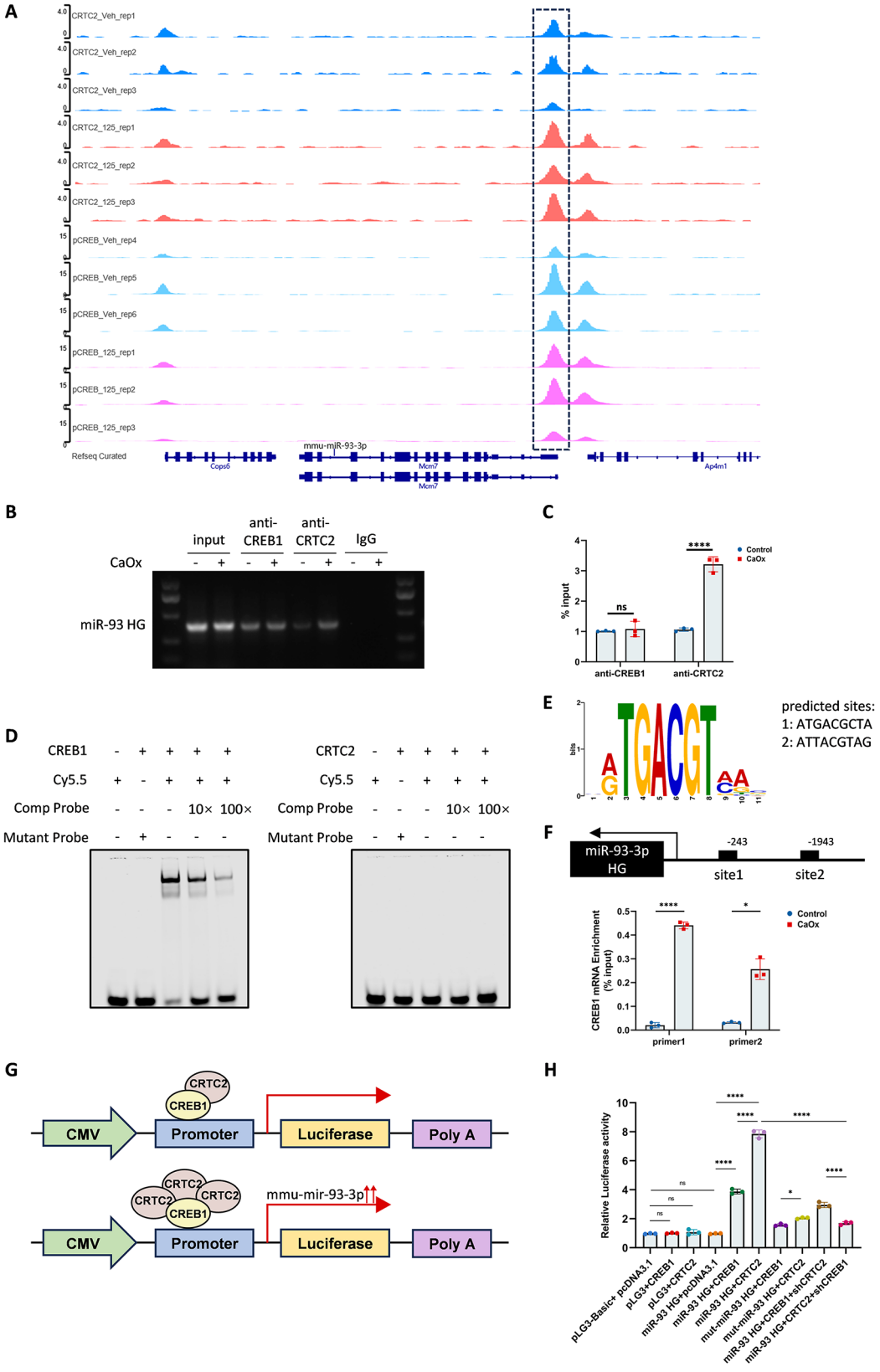

Fig. 8 (See legend on next page.)

(See figure on previous page.)

Fig. 8 miR-93-3p is specifically down-regulated in TCMK-1 cells by the master transcription factor complex CREB1/CRTC2. **A** CHIP-seq of 1,25(OH)2D_3 modelled C57BL/6J mice in GSE206777. Both p-CREB1 and CRTC2 were enriched at the upstream of promoter of miR-93 host gene (miR-93 HG). **B**-**C** Enrichment of CREB1 and CRTC2 on miR-93 HG. **D** Electrophoretic mobility shift assay (EMSA) for the analysis of CREB1 and CRTC2 binding on miR-93 HG promoter region. **E**-**F** Chip-qPCR assays of CREB1 in the promoter region of miR-93 HG in TCMK-1 cells. **G** A schematic diagram shows the structure of the luciferase reporter plasmid. Luciferase activity was enhanced when the CREB1/CRTC2 complex was increased. **H** Luciferase assay showed the effect on the luciferase activity of cells when transfected with different plasmids. Data are shown as mean ± SEM. P-values were calculated from two-tailed independent t-tests. One-way ANOVA with Tukey's multiple comparisons test.*$p < 0.05$, **$p < 0.01$, ***$p < 0.001$, ****$p < 0.0001$.

To investigate the role of exosomes on stone formation, exosomes were collected from TCMK-1 in the presence or absence of CaOx stimulation and labelled with DIR dye. 1 mg of exosomes was intravenously injected into each mouse once a week. Small animal in vivo imaging was performed 48 h later to observe the fluorescence signal in vivo.

The micrOFF mmu-miR-93-3p antagomir (RIBOBIO, China) was used to explore the effect of miR-93-3p on renal injury induced by kidney stones by tail intravenous injection once a week.

AAV9 virus injection

The AAV9 virus was provided by Designgene. Briefly, male mice were anesthetized with sodium pentobarbital 30 mg/kg intraperitoneally. and were injected with 1.5×10^{12} vg/ml AAV9-CMV-NFAT5-3×flag-ZsGreen and 1.5×10^{12} vg/ml AAV9- ZsGreen control into 5 different sites (10 μl at each site) of the renal parenchyma with a glass microliter syringe.

Drug treatment

To investigate the role of NIK on kidney injury caused by stones in mice, 60 mg/kg NIK SMI1 (Sigma Aldrich, German) was administered daily by gavage. The control group was given an equal amount of corn oil.

To investigate the relationship between METs and macrophage polarization, mice were subcutaneously injected daily with 10 mg/kg CI-amidine or PBS as controls.

Cell culture and treatment

TCMK-1 cells were cultured in DMEM medium containing 10% fetal bovine serum (FBS, Vivacell, China) and 1% Penicillin- Streptomycin-Amphotericin B Solution at 37℃, 5% CO2. According to the previous study, the cells were treated with 100 μg/ml calcium oxalate monohydrate (COM) for 24 h to establish an in vitro stone model. TCMK-1 cells were pretreated with 10 μM GW4869 or transfected with miR-93-3p mimics, miR-93-3p inhibitors, and negative control (RIBOBIO, Guangzhou).

The NAFT5 overexpressed lentivirus (LV-NFAT5, Genechem, China) was transferred into RAW264.7, to construct stable transfected cell lines. The component order of the overexpression vector was pLVX-NFAT5 -3×Flag-zsgreen-Puro.

Expression plasmids Flag-NFAT5, His-NIK, Myc-cIAP1/2, and HA-UB, and si-NIK and si-NFAT5, all purchased from Designgene. siRNAs and plasmids were transfected into RAW264.7 cells using Lipofectamine™2000 according to the manufacturer's instructions. The sequences are listed in Table S2.

Exosome isolation and characterization

The culture medium supernatant of TCMK-1 cells was collected and centrifuged several times according to the procedure described in previous articles [43]. In shourt, total RNA was extracted using an miRNeasy Micro Kit (217084, Qiagen, Germany) according to the manufacturer's protocol. The quantity and quality of the RNA were determined using the RNA ScreenTape assay on an Agilent 4200 TapeStation system (Agilent, CA, USA). The exosomes obtained were resuspended in PBS for subsequent experiments.

Nanoparticle tracking analysis (NTA) was used to evaluate the size and concentration of exosomes. Mouse kidney samples were fixed with 1% glutaraldehyde in PBS and subsequently used the transmission electron microscopy (TEM, HT7500, Hitachi, Japan) to observe morphology and size of exosomes.

Exosome tracing assay

TCMK-1-derived exosomes were treated with PKH26 (Umibio, China) were incubated for 10 min and washed with PBS to remove unbound PKH26. RAW264.7 cells were then incubated with PKH26-labelled exosomes (3.5×10^7 particles/mL) for 24 h.

For in vivo experiments, exosomes were labelled by DIR (Umibio, China) for 30 min, and were delivered into mice by tail intravenous injection. The distribution of exosomes in vivo was observed by in vivo imaging.

MiRNA sequencing

miRNA library preparation of CaOx-exo and Ctrl-exo for high-throughput sequencing was conducted by a QIAseq miRNA Library Kit(Qiagen, Germany). Briefly, the library was quantified by High Sensitivity DNA Kit using Agilent. Then, the libraries were diluted as required and sequenced using the Illumina Nova seq platform (Illumina, San Diego, CA, USA). The quality of the RNA-seq data was assessed by FastQC. The clean reads were mapped to the database of miRbase using Bowtie software and assigned to miRNA biotypes and analysis were performed by Wayen Biotechnologies (Shanghai, China). We used DEGseq to identify differentially expressed

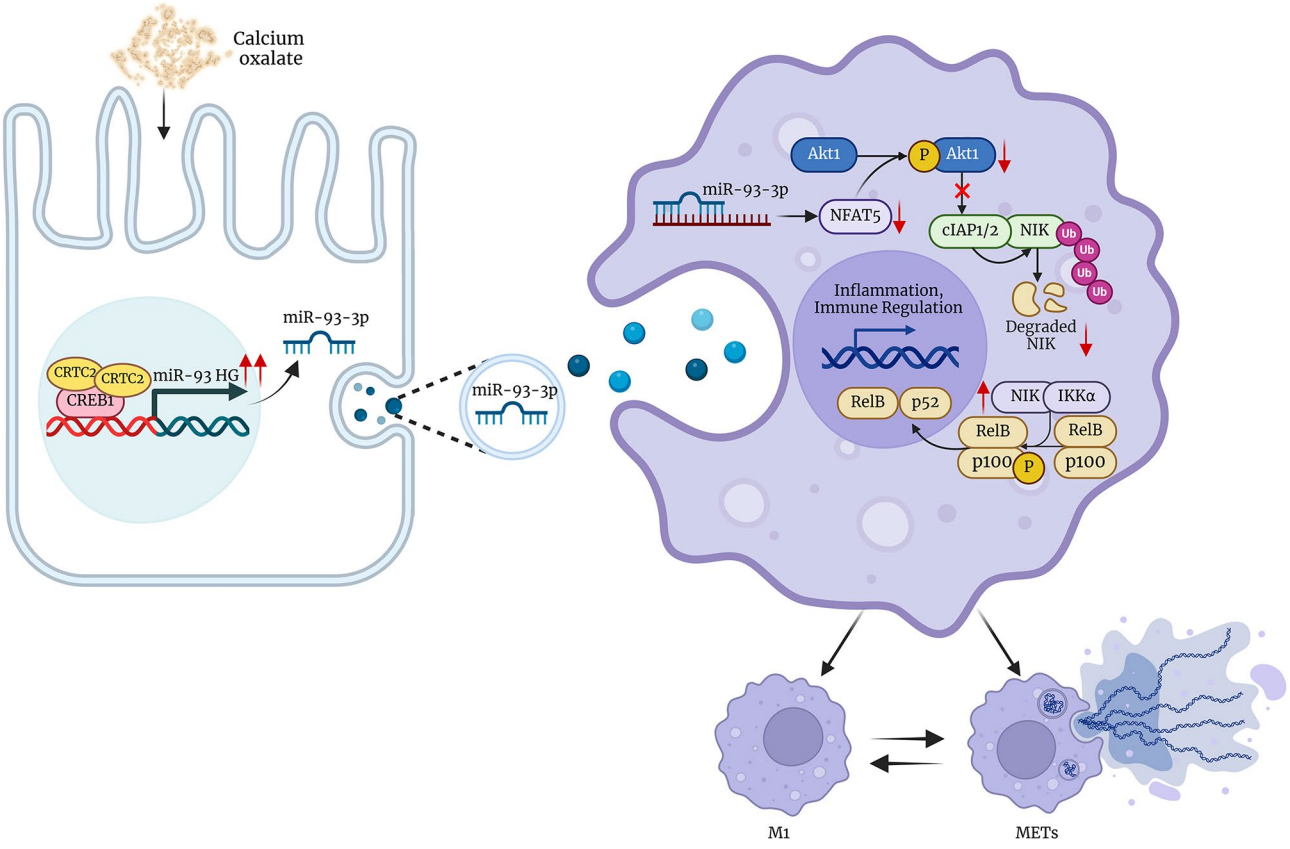

Fig. 9 Schematic of the mechanism of CaOx-exo in renal injury caused by kidney stones. CaOx-exo activates Akt1/NIK/ NF-κB2 pathway through miR-93-3p/NFAT5 axis to promote the M1 polarization and the formation of METs, thereby promoting the progression of kidney injury

miRNAs in exosomes. Subsequently, bioinformatics analyses was perfromed by OmicStudio tools (https://www.omicstudio.cn/tool).

RNA-sequencing (RNA-seq)

CaOx-exo and Ctrl-exo treated macrophages were subjected to high-throughput RNA sequencing (Wayenbiotech, China). DEGseq was used to identify differentially expressed genes in macrophages and enrichment analysis was performed(SeqHealth, Wuhan).

ELISA

The levels of IL-6, IL-8, TNF-α and IL-10 were measured by ELISA kits(Beyotime Biotechnology, China).

Western blot

Kidney tissues and cells were treated with RIPA buffer (Servicebio, China). Protein samples were then subjected to 10% or 7.5% SDS-PAGE and transferred to a PVDF membrane. After sealing with 5% skimmed milk, the membrane was incubated with primary antibody at 4 °C overnight. After washing 3 times, the membrane was incubated with secondary antibody (sheep anti-mouse IgG or sheep anti-rabbit IgG) for 1 h at room temperature. Bands were acquired using the Bio-Rad ChemiDoc™ Touch Imaging System, USA. Semi-quantitative analysis of the examples was performed by ImageJ. Details of antibodies used are shown in Table S3.

qRT–PCR

RNA was extracted from mouse kidney tissue and TCMK-1 or macrophages using VeZol reagent (R411-01, Vazyme). cDNA is produced by reverse transcription, using a reverse transcription kit (G3333-50, Servicebio), and gene expression levels were measured using ABscript Neo RT master Mix (RK20433, Abclonal). The primers are shown in Table S4.

Flow cytometry

Briefly, fixed and permeabilized RAW264.7 were performed using FIX & PERM™ Cell Permeabilization Kit (GAS003, Thermo Fisher) for different treatments. Then, FITC- conjugated anti-F4/80 and PE-conjugated anti-iNOS were used to label RAW264.7. Stained cells were collected and analyzed by flow cytometry (Beckman 270 Coulter Life Sciences, China). FlowJo software (version 10.8.1) was used to analyze the results.

Immunofluorescence (IF) staining

For cellular immunofluorescence staining, fixed cells on slides were washed three times with cold PBS. Then fix slides with 4% paraformaldehyde for 20 min at room temperature. Next, cells were permeabilized with 0.5% Triton X-100, blocked with 3% goat serum for 2 h, and then incubated with primary antibodies overnight. Images were taken using a fluorescence microscope (Olympus FV1200, Japan). Antibodies are listed in Table S3.

Immunohistochemistry (IHC)

Mouse kidney sections weighing 5 mm were deparaffinized, rehydrated, repaired, and treated in 3% H2O2 for 10 min. Trials were performed according to our previous procedures. The antibodies used are listed in Table S3.

CO-IP

TCMK-1 cells were cotransfected with the desired plasmid, and cell lysates were obtained by IP lysis buffer. Samples were incubated with 2 to 5 μg of His antibody overnight at 4 °C. Protein A/G beads were then added and incubated overnight at 4 °C. They were washed 3 times with elution buffer, resuspended in SDS loading buffer, and heated at 95 °C for 10 min before immunoblot analysis. The level of ubiquitination was determined by immunoblotting with anti-HA antibody.

Luciferase reporter assay

To construct the luciferase reporter, the WT NAFT5 3'utr and MT NAFT5 3'utr containing the miR-93-3p binding site were constructed and inserted into the pmirGLO vector. The pmirGLO vector contained Firefly luciferase and Renilla luciferase, and Renilla luciferase was used as a control. The luciferase reporter gene and miR-93-3p mimics or control were co-transfected into RAW264.7 using Lipofectamine 2000. After 36 h of culture, luciferase activity was measured by Fluorescence detector.

Chromatin Immunoprecipitation (ChIP)-sequence and CHIP-qPCR

Briefly, cells were fixed with 1% formaldehyde, and subsequent samples were prepared using the ChIP Assay Kit (Beyotime, China). The protein-DNA complexes were incubated with antibodies overnight at 4 °C. The obtained DNA was eluted, reverse cross-linked, purified, and finally samples were analyzed by agarose gel electrophoresis and qRT-PCR. The primer sequences used are shown in Table S5.

Electrophoretic mobility shift assay (EMSA)

The purified CREB1 and CRTC2 proteins were from Sinobiological (China). Double-stranded DNA probes (final concentration 20 nM) were labelled with Cy5.5 fluorescein at 5 ', incubated with purified protein in buffer, loaded onto prefabricated low-concentration in situ polyacrylamide gels, and separated protein-DNA complexes and free probes by electrophoresis at low temperature. Binding complexes and free probes were detected by fluorescence imaging to determine the binding and specificity of the protein to DNA.

Macrophage extracellular traps (METs) identification assays

RAW264.7 cells were pretreated with METs inhibitor CI-amidine or inducer Ionomycin for 24 h, and cells that developed METosis were labelled with MMP12 and citH3. By staining with SYTOX-green (KeyGENBioTech, China), the morphology and number of METs could be observed under the fluorescence microscope.

Statistical analyses

Statistical analysis was performed using GraphPad Prism 9. Continuous variables were expressed as mean ± standard deviation (SD). The normality of the data was assessed using the Shapiro-Wilk test and homogeneity of variances was verified with Levene's test. For comparisons between two groups, an independent-sample Student's t-test was employed. For comparisons of more than two groups, one-way analysis of variance (ANOVA) was used to evaluate significant differences in the means and post hoc multiple comparisons were performed using the Tukey-Kramer test. A p-value < 0.05 was considered statistically significant.

Supplementary Information

The online version contains supplementary material available at https://doi.org/10.1186/s12951-025-03246-9.

Supplementary Material 1

Supplementary Material 2: Fig. S1. (A) Quantitative analysis of relative fluorescence intensity in Fig. 3.H shows the expression levels of iNOS in the indicated groups in RAW264.7 cells. (B) Quantitative analysis of relative fluorescence intensity in Fig. 3.I shows the expression levels of TSG101 and iNOS in the indicated groups in mouse kidneys. (C) Rab27a knockout was confirmed by PCR (target allele: 651 bp; internal control product size: 335 bp). (D) Statistical results of the relative fluorescence intensities of TSG101 and iNOS in Fig. 2I. Data are shown as mean ± SEM. One-way ANOVA with Tukey's multiple comparisons test. *$p < 0.05$, **$p < 0.01$, ***$p < 0.001$, ****$p < 0.0001$

Supplementary Material 3: Fig. S2. A. GO enrichment of the RNA sequencing results of CaOx-exo and Ctrl-exo-treated macrophages. B-C. Quantitative analysis of Western blot bands in Fig. 3E-F. D. Quantitative analysis of Western blot bands in Fig. 3L shows the expression levels of NFAT5 and iNOS in kidneys of mice and human. Data are shown as mean ± SEM. One-way ANOVA with Tukey's multiple comparisons test. P-values were calculated from two-tailed independent t-tests. *$p < 0.05$, **$p < 0.01$, ***$p < 0.001$, ****$p < 0.0001$

Supplementary Material 4: Fig. S3. (A) Mean MAP3K14(NIK) expression levels were measured at multiple time points during 28 days of IRI and 14 days of UUO. (B) Single-cell sequencing was used to analyze the expression level of NIK in each cell of the fibrotic kidneys. Data were obtained from the Mouse kidney uni-IRI and UUO time courses profiled with sci-RNA-seq3 dataset of the KIT database (http://humphreyslab.com/Sin

gleCell/)

Supplementary Material 5: Fig. S4. (A) Western blot bands and quantification of His and p-Akt1 levels with the usage of transfected SC79 of indicated concentrations after transfecting His-NIK plasmid in RAW264.7 cells. (B) p-Akt1 reduced the stability of NIK. C.Post-translational modification sites of NIK were obtained from the PhosphoSitePlus database. D. Co-immunoprecipitation results for NIK and p-Akt1. E. Effect of SC79 treatment on NF-κB2 pathway in RAW264.7 cells transfected with His-NIK plasmid. Data are shown as mean ± SEM. In A, P-values were calculated from two-tailed independent t-tests. In E, two-way ANOVA followed by Tukey's post-test. *$p < 0.05$, **$p < 0.01$, ***$p < 0.001$, ****$p < 0.0001$

Supplementary Material 6: Fig. S5. (A) Fluorescence images of lungs, livers and kidneys were obtained at 6 h, 12 h, 24 h and 48 h after tail intravenous injection into mice of DIR-labelled exosomes derived from TCMK-1. (B) Fluorescence images of kidneys were obtained at 6 h, 12 h, 24 h and 48 h after tail intravenous injection into mice of DIR-labelled exosomes derived from TCMK-1

Supplementary Material 7

Graphical Abstract

Table S1

Table S2

Table S3

Table S4

Table S5

Acknowledgements
This study was supported by grant from National Natural Science Foundation of (82100806,82270802,82170775,82370765), The Open Project of Hubei Key Laboratory 2023KFZZ009 and The Fundamental Research Funds for the Central Universities 2042023kf0022.

Author contributions
YSS, BJL, and FYL designed research; BFS and YQX performed research; TR analyzed data; XJZ and FC wrote the paper. All authors reviewed the manuscript.

Funding
This study was supported by grant from National Natural Science Foundation of (82100806, 82270802, 82170775, 82370765), The Open Project of Hubei Key Laboratory 2023KFZZ009 and The Fundamental Research Funds for the Central Universities 2042023kf0022.

Data availability
No datasets were generated or analysed during the current study.

Declarations

Ethics approval and consent to participate
The study protocol involving human tissues adhered to the Declaration of Helsinki and was approved by the review board of Renmin Hospital of Wuhan University (WDRY2021-KS047). All treatments of animals were approved by the Animal Welfare and Ethics Committee of the People's Hospital of Wuhan University (approval number: WDRM20200604). The authors declare no competing interests.

Competing interests
The authors declare no competing interests.

Author details
[1]Department of Urology, Renmin Hospital of Wuhan University, No. 238 Jiefang Road, Wuchang District, Wuhan, Hubei 430060, P.R. China

Received: 10 December 2024 / Accepted: 18 February 2025
Published online: 12 March 2025

References

1. Khan SR, Pearle MS, Robertson WG, Gambaro G, Canales BK, Doizi S, et al. Kidney stones. Nat Reviews Disease Primers. 2016;2:16008.
2. Thongprayoon C, Krambeck AE, Rule AD. Determining the true burden of kidney stone disease. Nat Rev Nephrol. 2020;16(12):736–46.
3. Siener R. Nutrition and kidney stone disease. Nutrients. 2021;13(6).
4. Khan SR, Canales BK, Dominguez-Gutierrez PR. Randall's plaque and calcium oxalate stone formation: role for immunity and inflammation. Nat Rev Nephrol. 2021;17(6):417–33.
5. Sakhaee K. Exploring the role of inflammation toward the pathogenesis of calcium nephrolithiasis. Clin J Am Soc Nephrology: CJASN. 2022;17(3):338–9.
6. Kusmartsev S, Dominguez-Gutierrez PR, Canales BK, Bird VG, Vieweg J, Khan SR. Calcium oxalate stone fragment and crystal phagocytosis by human macrophages. J Urol. 2016;195(4 Pt 1):1143–51.
7. Liu Q, Liu Y, Guan X, Wu J, He Z, Kang J, et al. Effect of M2 macrophages on injury and apoptosis of renal tubular epithelial cells induced by calcium oxalate crystals. Kidney Blood Press Res. 2019;44(4):777–91.
8. Wen Y, Lu X, Ren J, Privratsky JR, Yang B, Rudemiller NP, et al. KLF4 in macrophages attenuates TNFα-Mediated kidney injury and fibrosis. J Am Soc Nephrology: JASN. 2019;30(10):1925–38.
9. Kormann R, Kavvadas P, Placier S, Vandermeersch S, Dorison A, Dussaule JC, et al. Periostin promotes cell proliferation and macrophage polarization to drive repair after AKI. J Am Soc Nephrology: JASN. 2020;31(1):85–100.
10. Yunna C, Mengru H, Lei W, Weidong C. Macrophage M1/M2 polarization. Eur J Pharmacol. 2020;877:173090.
11. Okada A, Yasui T, Fujii Y, Niimi K, Hamamoto S, Hirose M, et al. Renal macrophage migration and crystal phagocytosis via inflammatory-related gene expression during kidney stone formation and elimination in mice: detection by association analysis of stone-related gene expression and microstructural observation. J Bone Mineral Research: Official J Am Soc Bone Mineral Res. 2010;25(12):2701–11.
12. Tsujihata M. Mechanism of calcium oxalate renal stone formation and renal tubular cell injury. Int J Urology: Official J Japanese Urol Association. 2008;15(2):115–20.
13. Liu H, Yang X, Tang K, Ye T, Duan C, Lv P, et al. Sulforaphane elicts dual therapeutic effects on renal inflammatory injury and crystal deposition in calcium oxalate nephrocalcinosis. Theranostics. 2020;10(16):7319–34.
14. Gu W, Huang C, Chen G, Kong W, Zhao L, Jie H, et al. The role of extracellular traps released by neutrophils, eosinophils, and macrophages in asthma. Respir Res. 2024;25(1):290.
15. Huang X, Yi N, Zhu P, Gao J, Lv J. Sorafenib-induced macrophage extracellular traps via ARHGDIG/IL4/PADI4 axis confer drug resistance through inhibiting ferroptosis in hepatocellular carcinoma. Biol Direct. 2024;19(1):110.
16. Sun Z, Zhang F, Gao Z, Wu J, Bi Q, Zheng X, et al. Liraglutide alleviates ferroptosis in renal ischemia reperfusion injury via inhibiting macrophage extracellular trap formation. Int Immunopharmacol. 2024;142Pt B:113258.
17. Ludwig N, Whiteside TL, Reichert TE. Challenges in exosome isolation and analysis in health and disease. Int J Mol Sci. 2019;20(19).
18. He C, Zheng S, Luo Y, Wang B. Exosome theranostics: biology and translational medicine. Theranostics. 2018;8(1):237–55.
19. Zhang J, Li S, Li L, Li M, Guo C, Yao J, et al. Exosome and Exosomal MicroRNA: trafficking, sorting, and function. Genom Proteom Bioinform. 2015;13(1):17–24.
20. Yang B, Chen Y, Shi J. Exosome Biochemistry and advanced nanotechnology for next-generation theranostic platforms. Advanced materials (Deerfield Beach, Fla). 2019;31(2):e1802896.
21. Noonin C, Thongboonkerd V. Exosome-inflammasome crosstalk and their roles in inflammatory responses. Theranostics. 2021;11(9):4436–51.
22. Ståhl AL, Johansson K, Mossberg M, Kahn R, Karpman D. Exosomes and microvesicles in normal physiology, pathophysiology, and renal diseases. Pediatric nephrology (Berlin, Germany). 2019;34(1):11–30.
23. Sun Y, Li B, Zhou X, Rao T, Cheng F. The identification of key molecules and pathways in the crosstalk of calcium oxalate-treated TCMK-1 cells and macrophage via exosomes. Sci Rep. 2024;14(1):20949.
24. Wang Q, Sun Y, Yang Y, Li C, Zhang J, Wang S. Quantitative proteomic analysis of urinary exosomes in kidney stone patients. Translational Androl Urol. 2020;9(4):1572–84.
25. Mo L, Huang H-Y, Zhu X-H, Shapiro E, Hasty DL, Wu X-R. Tamm-Horsfall protein is a critical renal defense factor protecting against calcium oxalate crystal formation. Kidney Int. 2004;66(3):1159–66.

26. Poggio M, Hu T, Pai C-C, Chu B, Belair CD, Chang A et al. Suppression of Exosomal PD-L1 induces systemic Anti-tumor immunity and memory. Cell. 2019;177(2).
27. Zhou Y, Zhang Y, Xu J, Wang Y, Yang Y, Wang W, et al. Schwann cell-derived exosomes promote lung cancer progression via miRNA-21-5p. Glia. 2024;72(4):692–707.
28. Li M, Kim Y-M, Koh JH, Park J, Kwon HM, Park J-H et al. Serum amyloid A expression in liver promotes synovial macrophage activation and chronic arthritis via NFAT5. J Clin Invest. 2024;134(5).
29. Li H, Dixon EE, Wu H, Humphreys BD. Comprehensive single-cell transcriptional profiling defines shared and unique epithelial injury responses during kidney fibrosis. Cell Metab. 2022;34(12).
30. Lin L, Yu H, Li L, Yang W, Chen X, Gong Y, et al. TRIM55 promotes noncanonical NF-κB signaling and B cell-mediated immune responses by coordinating p100 ubiquitination and processing. Sci Signal. 2023;16(806):eabn5410.
31. Zhang J, Webster JD, Dugger DL, Goncharov T, Roose-Girma M, Hung J et al. Ubiquitin ligases cIAP1 and cIAP2 limit cell death to prevent inflammation. Cell Rep. 2019;27(9).
32. Kamerkar S, Leng C, Burenkova O, Jang SC, McCoy C, Zhang K, et al. Exosome-mediated genetic reprogramming of tumor-associated macrophages by exoASO-STAT6 leads to potent monotherapy antitumor activity. Sci Adv. 2022;8(7):eabj7002.
33. Xun Y, Zhou P, Yang Y, Li C, Zhang J, Hu H, et al. Role of Nox4 in high Calcium-Induced renal oxidative stress damage and crystal deposition. Antioxid Redox Signal. 2022;36(1–3):15–38.
34. Dong C, Zhou J, Su X, He Z, Song Q, Song C, et al. Understanding formation processes of calcareous nephrolithiasis in renal interstitium and tubule lumen. J Cell Mol Med. 2024;28(7):e18235.
35. Zhou X, Zhao S, Li W, Ruan Y, Yuan R, Ning J, et al. Tubular cell-derived Exosomal miR-150-5p contributes to renal fibrosis following unilateral ischemia-reperfusion injury by activating fibroblast in vitro and in vivo. Int J Biol Sci. 2021;17(14):4021–33.
36. Yang X, Liu H, Ye T, Duan C, Lv P, Wu X, et al. AhR activation attenuates calcium oxalate nephrocalcinosis by diminishing M1 macrophage polarization and promoting M2 macrophage polarization. Theranostics. 2020;10(26):12011–25.
37. He J, Cao Y, Zhu Q, Wang X, Cheng G, Wang Q et al. Renal macrophages monitor and remove particles from urine to prevent tubule obstruction. Immunity. 2024;57(1).
38. Zhu W, Zhao Z, Chou F, Zuo L, Liu T, Yeh S, et al. Loss of the androgen receptor suppresses intrarenal calcium oxalate crystals deposition via altering macrophage recruitment/M2 polarization with change of the miR-185-5p/CSF-1 signals. Cell Death Dis. 2019;10(4):275.
39. Zhu W, Qiong D, Changzhi X, Meiyu J, Hui L. Macrophage polarization regulation shed lights on immunotherapy for CaOx kidney stone disease. Biomed Pharmacother. 2024;179:117336.
40. Zhu W, Wu C, Zhou Z, Zhang G, Luo L, Liu Y, et al. Acetate attenuates hyperoxaluria-induced kidney injury by inhibiting macrophage infiltration via the miR-493-3p/MIF axis. Commun Biol. 2023;6(1):270.
41. Zhang Y, Liu Y, Liu H, Tang WH. Exosomes: biogenesis, biologic function and clinical potential. Cell Biosci. 2019;9:19.
42. Song DH, Lee JS, Lee J-H, Kim DC, Yang JW, Kim MH, et al. Exosome-mediated secretion of miR-127-3p regulated by RAB27A accelerates metastasis in renal cell carcinoma. Cancer Cell Int. 2024;24(1):153.
43. Zhao S, Li W, Yu W, Rao T, Li H, Ruan Y, et al. Exosomal miR-21 from tubular cells contributes to renal fibrosis by activating fibroblasts via targeting PTEN in obstructed kidneys. Theranostics. 2021;11(18):8660–73.
44. Yang Y, Hong S, Wang Q, Wang S, Xun Y. Exosome-mediated crosstalk between epithelial cells amplifies the cell injury cascade in CaOx stone formation. J Biol Eng. 2023;17(1):16.
45. Zhu W, Zhou Z, Wu C, Huang Z, Zhao R, Wang X, et al. miR-148b-5p regulates hypercalciuria and calcium-containing nephrolithiasis. Cell Mol Life Sci. 2024;81(1):369.
47. Zhang W, Liao Y, Lou J, Zhuang M, Yan H, Li Q, et al. CircRNA_Maml2 promotes the proliferation and migration of intestinal epithelial cells after severe burns by regulating the miR-93-3p/FZD7/Wnt/β-catenin pathway. Burns Trauma. 2022;10:tkac009.
48. Du Y, Kong C. STAT3 regulates miR93-mediated apoptosis through inhibiting DAPK1 in renal cell carcinoma. Cancer Gene Ther. 2021;28(5):502–13.
49. Feng Z, Chen R, Huang N, Luo C. Long non-coding RNA ASMTL-AS1 inhibits tumor growth and Glycolysis by regulating the miR-93-3p/miR-660/FOXO1 axis in papillary thyroid carcinoma. Life Sci. 2020;244:117298.
50. Choi SY, Lee-Kwon W, Kwon HM. The evolving role of TonEBP as an immunometabolic stress protein. Nat Rev Nephrol. 2020;16(6):352–64.
51. Yoo EJ, Oh K-H, Piao H, Kang HJ, Jeong GW, Park H, et al. Macrophage transcription factor TonEBP promotes systemic lupus erythematosus and kidney injury via damage-induced signaling pathways. Kidney Int. 2023;104(1):163–80.
52. Xu J, Gao C, He Y, Fang X, Sun D, Peng Z, et al. NLRC3 expression in macrophage impairs Glycolysis and host immune defense by modulating the NF-κB-NFAT5 complex during septic immunosuppression. Mol Ther. 2023;31(1):154–73.
53. Thongboonkerd V, Yasui T, Khan SR. Editorial: immunity and inflammatory response in kidney stone disease. Front Immunol. 2021;12:795559.
54. Karin M, Lin A. NF-kappaB at the crossroads of life and death. Nat Immunol. 2002;3(3):221–7.
55. Sun S-C. The noncanonical NF-κB pathway. Immunol Rev. 2012;246(1):125–40.
56. Basak S, Hoffmann A. Crosstalk via the NF-kappaB signaling system. Cytokine Growth Factor Rev. 2008;19(3–4):187–97.
57. Goncharov T, Niessen K, de Almagro MC, Izrael-Tomasevic A, Fedorova AV, Varfolomeev E, et al. OTUB1 modulates c-IAP1 stability to regulate signalling pathways. EMBO J. 2013;32(8):1103–14.
58. Yang X-D, Sun S-C. Targeting signaling factors for degradation, an emerging mechanism for TRAF functions. Immunol Rev. 2015;266(1):56–71.
59. Han MH, Lee WS, Jung JH, Jeong J-H, Park C, Kim HJ, et al. Polyphenols isolated from Allium cepa L. induces apoptosis by suppressing IAP-1 through inhibiting PI3K/Akt signaling pathways in human leukemic cells. Food Chem Toxicol. 2013;62:382–9.
60. Wang B, Hu S, Teng Y, Chen J, Wang H, Xu Y, et al. Current advance of nanotechnology in diagnosis and treatment for malignant tumors. Signal Transduct Target Ther. 2024;9(1):200.
61. Gianvincenzo PD, Leyes MF, Boonkam K, Puentes AF, Reyes SG, Nardi AN, et al. Supramolecular citrate Poly Allylamine hydrochloride nanoparticles for citrate delivery and calcium oxalate nanocrystal dissolution. J Colloid Interface Sci. 2024;669:667–78.
62. Vu TD, Sohng W, Jang E, Choi D, Chung H. Feasibility of discrimination of gall bladder (GB) stone and GB polyp using voltage-applied SERS measurement of bile juice samples in conjunction with two-trace two-dimensional (2T2D) correlation analysis. Analyst. 2021;146(3):1091–8.
63. Zhao Y, Pu M, Wang Y, Yu L, Song X, He Z. Application of nanotechnology in acute kidney injury: from diagnosis to therapeutic implications. J Control Release. 2021;336:233–51.
64. Yu H, Jin F, Liu D, Shu G, Wang X, Qi J, et al. ROS-responsive nano-drug delivery system combining mitochondria-targeting ceria nanoparticles with Atorvastatin for acute kidney injury. Theranostics. 2020;10(5):2342–57.

Publisher's note